Coupled Oscillation

Jordan Walsh - 120387836

Off-Campus Practical Report – PY3107

University College Cork

Department of Physics

January 2023 – March 2023

Coupled Oscillation

1. Introduction

This report details 5 total experiments focused on coupled oscillation. These experiments were 'take-home' experiments, the first 3 of which (*a – c*) had the purpose of obtaining fundamental and necessary constants for the latter, which are an investigation and measurement of 'beats'– "*pulsation caused by the combination of two waves of slightly different frequencies*" [1] - and Parametric Resonance.

1.1 Overview

There are 5 Experiments to discuss in this report:

(a) 'Free Cantilever Oscillations'
(b) 'Mass Suspended from Cantilever'
(c) 'Moments of Inertia and Torsional Oscillation'
(d) 'Coupled Masses on a Cantilever'
(e) 'Phone Oscillation Modes and Parametric Resonance'

1.1.1 Free Cantilever Oscillations (a)

In this experiment, a smart phone is used as a seismograph, detecting vibrations transmitted from a vibrating cantilever clamped to the worktop in use. From the data recorded, a number of constants will be determined, notably; the *Young's Modulus, E,* of the cantilever.

1.1.2 Mass Suspended from Cantilever (b)

The context for this section will be in terms of a spring-mass system suspended from the cantilever discussed previously. Here, the spring constants of the springs intended for experimental use will be determined and the Young's Modulus, *E*, of the cantilever will be determined by varying the point of suspension of the mass-spring system and compared to the result determined in Experiment (a).

1.1.3 Moments of Inertia and Torsional Oscillation (c)

The period of torsional oscillations, principal moments of inertia, and gyration radii will be determined for 2 objects (and each for both possible orientations respectively): A rectangular wooden block (by conventional timing methods) and a mobile phone (by using on-board magnetic sensor *[Phyphox]*).

1.1.4 Coupled Masses on a Cantilever (d)

This experiments investigates the phenomenon of 'beats', focussing on the frequencies of coupled modes (mass-spring systems in vertical oscillation) on the cantilever. This section also includes a brief additional investigation into the effects and dynamics of a double-mass spring (in series) on the cantilever.

1.1.5 Phone Oscillation Modes and Parametric Resonance (e)

Parametric resonance refers to coupling between pendulum motion and vertical oscillatory motion in an elastic pendulum as a result of non-linear resonance. In this experiment we investigate and identify the dynamics and vibrational modes of an elastic pendulum.

1.2 Equipment (All Experiments)

- A Smartphone (Running Phyphox – a measurement tool utilising various sensors on-board the phone developed at RWTH Physics Ins.). The smartphone was used at various points to obtain and record crucial data. The smartphone acted as a seismograph, accelerometer, magnetometer and performed Fourier Transforms (using an FFT algorithm) of the data before export.
- A set of seven 50 g hanging weights and holder.
- 2 helical springs.
- A half-metre stick (wood), which was used as the cantilever throughout.
- A standard (100mm) G-clamp for securing the cantilever to a bench/worktop.
- Rectangular MDF block.
- Block/Phone Holder custom made utilising the following provided materials:
    - Ziplock Plastic Bag
    - A4 cardboard sheet
    - 4 standard double picture hooks
- A length of cotton string

Experimental Methods

The following sections, detail the theory, procedure and experimental data produced from each experiment while providing brief discussion of reported data and fulfilling specified criteria of the lab brief.

2. Free Cantilever Oscillations (a)

2.1 Theory/Procedure

The oscillation frequency, *f*, of a uniform cantilever of length *L* is given by

$$f = \frac{\beta^2}{2\pi}\sqrt{\frac{EI}{m}}\frac{1}{L^2}$$

where $\beta \approx 1.875$ (the smallest possible solution to $\cos\beta\cosh\beta = -1$), *E* is the Young's Modulus of the cantilever, *I* is the second moment of cross section area and *m* is the mass per unit length. The second moment of cross section area is given by

$$I = \frac{Wt^3}{12}$$

where *W* and *t* are width and thickness of the cantilever (half-meter stick) respectively.

Fig 2.1 – Experimental Setup – Phone placed on worktop at base of half meter stick (phyphox)

The data for Experiment (a), as shown in section 2.2, was obtained as follows:

The cantilever (half-meter stick) was clamped to a bench as shown in Figure 2.1. The smartphone was placed on the top side of the bench laying face up as close the cantilever fixed point as possible. Data was acquired by running the acceleration spectrum in phyphox for approximately *5 seconds* and setting the cantilever into damped simple harmonic motion by deflecting the beam manually. This process was repeated for various cantilever lengths.

2.2 Experimental Data

Length		Peak Freq (f)		L^{-2}
m		Hz		m^{-2}
0.25	±0.005	75.1953	±0.7	16
0.3	±0.005	49.8074	±0.7	11.1111
0.32	±0.005	43.943	±0.7	9.76563
0.34	±0.005	40.039	±0.7	8.65052
0.36	±0.005	35.534	±0.7	7.71605
0.38	±0.005	32.226	±0.7	6.92521
0.39	±0.005	30.2734	±0.7	6.57462
0.4	±0.005	28.32	±0.7	6.25
0.41	±0.005	27.13	±0.7	5.94884
0.42	±0.005	26.367	±0.7	5.66893
0.43	±0.005	24.41	±0.7	5.40833
0.44	±0.005	23.341	±0.7	5.16529
0.45	±0.005	22.46	±0.7	4.93827

Tab 2.1 – Free Cantilever Oscillation Data

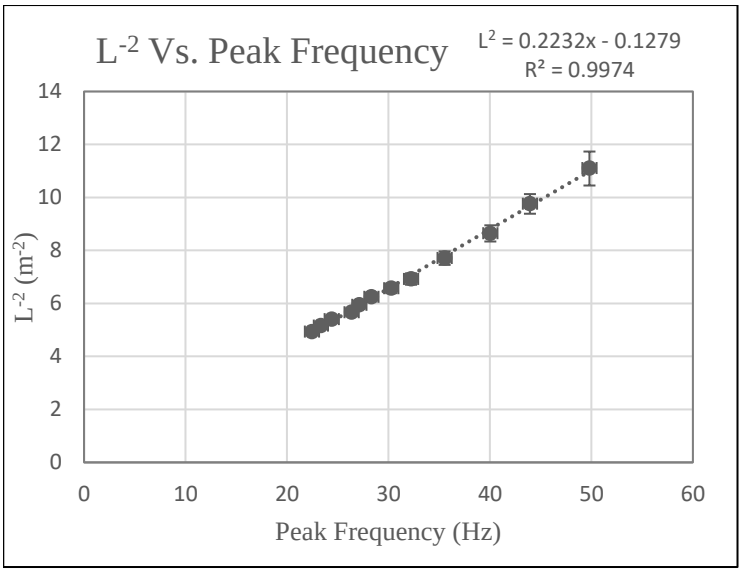

Fig 2.2 – Plotted Experimental data | s = 0.2232

2.3 Calculation / Error Analysis

Ruler Specifications				
Length	Width	Thickness	Mass	m
m	m	m	kg	kg m^{-1}
0.5	0.02545	0.00695	0.055762	0.111524
±0.01	±0.000005	±0.0002	±0.0000005	±0.000001

Tab 2.2 – Ruler Specifications

$s = 0.2232\ m^{-2}Hz^{-1},\ \ \Delta s = 0.003573715$ *(Fig 2.1 -* Δs *determined via Excel Regression Analysis)*

Second moment cross section area, *I*:

$$I = \frac{Wt^3}{12} = \frac{(0.02545\ m)(0.00695\ m)^3}{12} = 7.1197 \times 10^{-10}\ m^4$$

$$\frac{\Delta I}{I} = \frac{\Delta W}{W} + 3\frac{\Delta t}{t} = \frac{0.000005}{0.02545} + 3\frac{0.0002}{0.00695} = 0.0865274$$

$$\rightarrow\ \Delta I = (0.0865274)(7.1197 \times 10^{-10}\ m^4) = 0.61605 \times 10^{-10} m^4$$

$$\therefore\ \boldsymbol{I = (7.1 \pm 0.6) \times 10^{-10} m^4}$$

Young's Modulus of Cantilever, *E*:

$$f = \frac{\beta^2}{2\pi}\sqrt{\frac{EI}{m}}\frac{1}{L^2} \;\rightarrow\; E = \frac{(f^2L^4)4\pi^2 m}{\beta^4 I} = \frac{s^2 4\pi^2 m}{\beta^4 I}$$

$$\frac{s^2 4\pi^2 m}{\beta^4 I} = \frac{(0.630357\ m^{-2}Hz^{-1})^2 4\pi^2 (0.111524\ \text{kg})}{(1.875)^4(7.1197\times10^{-10}\ m^4)} = 1.0047\times10^{10}\ Nm^{-2}$$

$$\frac{\Delta E}{E} = 2\frac{\Delta s}{s} + \frac{\Delta I}{I} + \frac{\Delta m}{m} = 2\left(\frac{0.003573715}{0.223154306}\right) + 0.0865274 + \frac{0.000001}{0.111524} = 0.1185655$$

$$\rightarrow \Delta E = 0.12\times10^{10}\ Nm^2$$

$$\therefore \boldsymbol{E = (1.0 \pm 0.1)\times 10^{10}\ Nm^{-2}}$$

Specified factor *EI*:

$$E = \frac{s^2 4\pi^2 m}{\beta^4 I} \rightarrow EI = \frac{s^2 4\pi^2 m}{\beta^4}$$

$$\therefore EI = \frac{(0.630357\ m^{-2}Hz^{-1})^2 4\pi^2 (0.111524\ \text{kg})}{(1.875)^4} = 7.1533989\ Nm^2$$

$$\frac{\Delta EI}{EI} = 2\frac{\Delta s}{s} + \frac{\Delta m}{m} = 2\left(\frac{0.003573715}{0.223154306}\right) + \frac{0.000001}{0.111524} = 0.03203$$

$$\rightarrow \Delta EI = 0.2291234$$

$$\therefore \boldsymbol{EI = 7.2 \pm 0.2\ Nm^2}$$

Utilised Error Analysis Parameters					
$\frac{\Delta m}{m}$	**$\frac{\Delta W}{W}$**	**$\frac{\Delta t}{t}$**	**$\frac{\Delta I}{I}$**	**$\frac{\Delta E}{E}$**	**$\frac{\Delta EI}{EI}$**
8.96668E-06	0.00019646	0.02877698	0.0865274	0.1185655	0.03203

Tab 2.3 – Error Parameters (Inc. parameters from half meter stick)

2.4 Results

Based on the data collected (as shown in section 2.2) and the analysis in section 2.3, the results for Experiment (a) are as follows:

$$\boldsymbol{E = (1.0 \pm 0.1)\times 10^{10}\ Nm^{-2}}$$

$$\boldsymbol{I = (7.1 \pm 0.6)\times 10^{-10} m^4}$$

$$\boldsymbol{EI = 7.2 \pm 0.2\ Nm^2}$$

2.5 Further Analysis *(Lab Brief Part 2) / Discussion*

A final measurement (for *L = 45cm*) was recorded and exported to an external computer for further analysis of the raw data from the mobile's sensors. This data has been included with the submission of this report.

The lab brief states: *"In the FFT Spectrum data, identify the position of the maximum of the power spectrum and extract (copy) data for a few Hz on either side of the peak. Plotting experimental data and a Lorentzian peak function with peak position, f_{peak}, and width, Δ."*

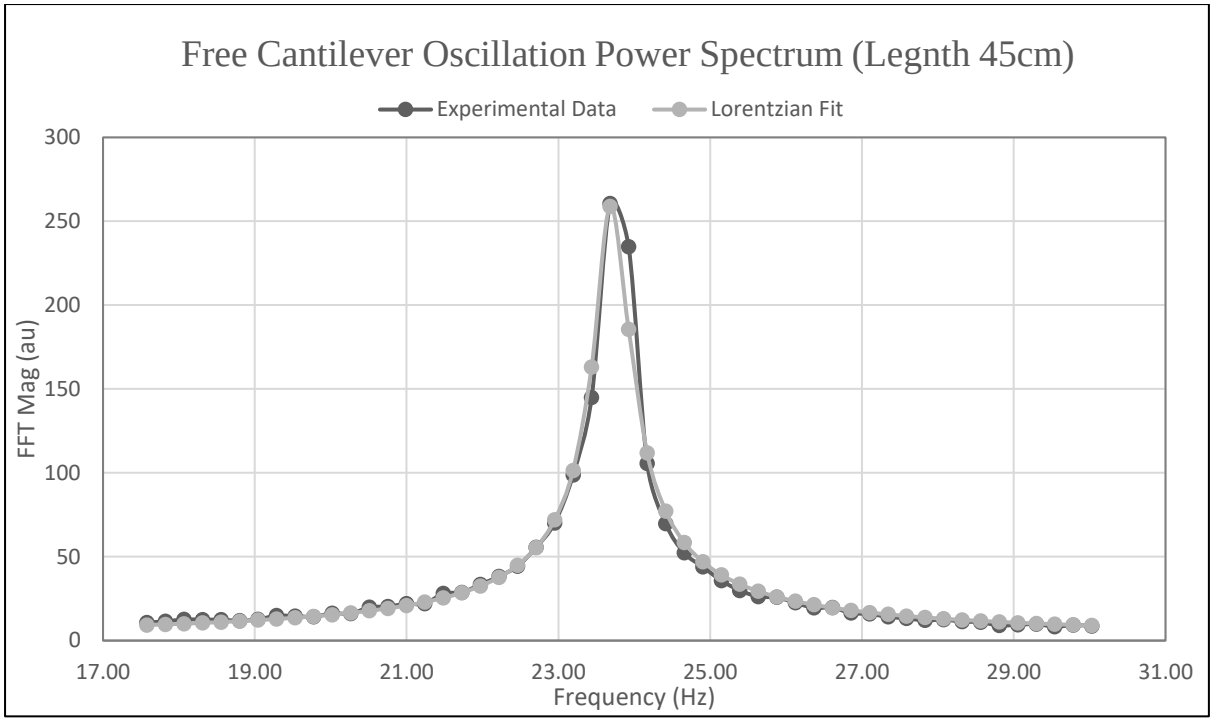

Fig 2.3 – Plotted FFT Spectrum and fitted Lorentzian as per lab brief

Variable Quantities		
A	Δ	**f_{peak}**
261.0812	2.18E-01	23.71
±6	±0.18	±0.2

Tab 2.4 – Lorentzian Parameters

The Lorentzian in Figure 2.3 was plotted using the Lorentzian function

$$P(f) = A\frac{\Delta}{\sqrt{(f - f_{peak})^2 + \Delta^2}}$$

where Δ is the Full Width at Half Maximum (FWHM), *A* is an arbitrary multiplier/amplitude and f_{peak} is the peak frequency as determined previously. The parameters were solved for using 'Solver', an Excel Package which allowed for constraints and variables to be appointed to solve a numerical problem. There was an attempt to improve the fit further '*by eye'.* This proved difficult so it was concluded that the solver had in fact found an optimal solution. The settled parameters are shown in Table 2.4. Interestingly, the peak frequency documented in the additional measurement differed (significantly) from that recorded in section 2.2 for the same cantilever length. I suspect the reason for this is due to a technical issue encountered during the experiment (*which was discussed in class*) in which the sampling rate of the device used for measurement was ~10 times that of what was trialled in the design of the lab brief procedure. This meant that the data points recorded from this device were more sparsely placed along a comparable region, as such effecting the results of section 2.4 negatively. The solution reached (before the solution provided at present was provided), was to increase the FFT sample number from 1024 to 4096 in order to achieve an appropriate number of samples from 0 – 50 Hz and thus also improving the accuracy of the data.

A section of the Raw acceleration data is shown in Figure 2.4, complete with **envelope functions fitted by eye**.

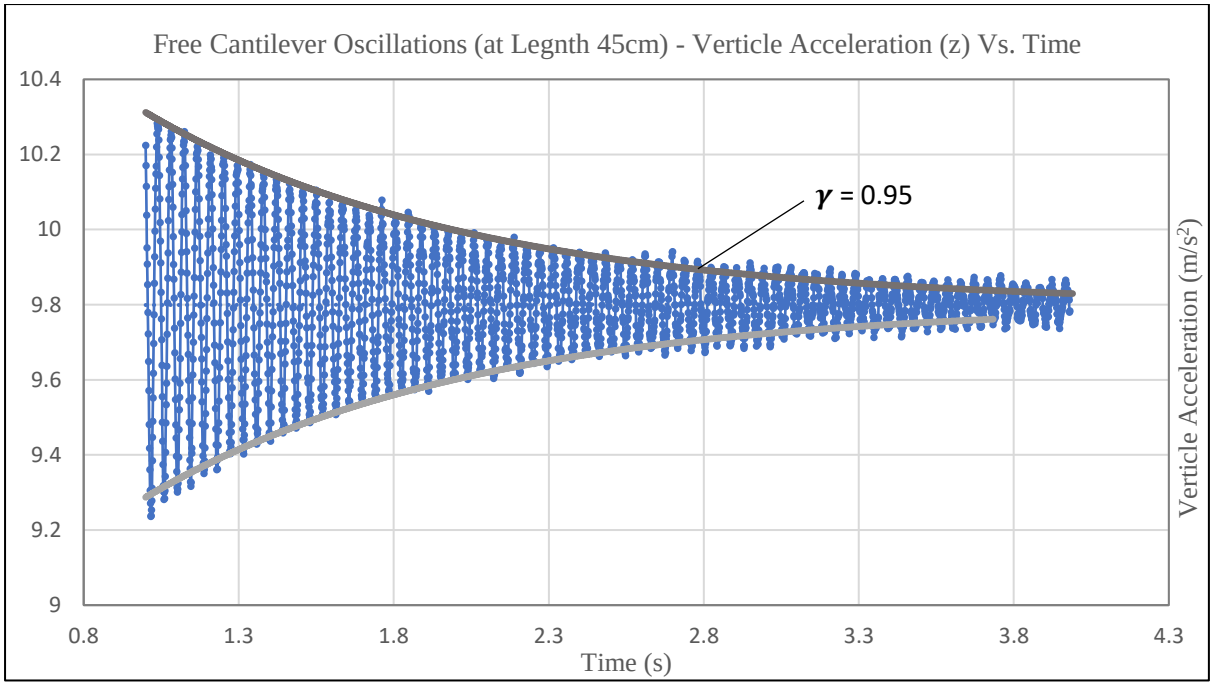

Fig 2.4 – Raw Acceleration data from smart-phone sensors – fitted with envelope functions. The decay rate of the exponentials was exactly γ = 0.95 – See submitted .xlsx file

$$\boldsymbol{\gamma = 0.95}$$

A damped exponential such as that formed by the raw data in Fig 2.4 is mathematically described by

$$z(t) = e^{-\gamma t}\cos(2\pi v t)$$

where γ is the damping factor, t represents time, and v is the proposed frequency of oscillation (this should be the peak frequency of the data in Fig 2.3). It has the following Fourier Transform:

$$P(f) = \frac{1}{2\pi\sqrt{(f-v)^2 + \left(\frac{\gamma}{2\pi}\right)^2}}$$

(*derivation in Appendix A.1*)

This is identical in form to the Lorentzian function plotted in Fig 2.3. $\frac{\gamma}{2\pi}$ as a factor should correspond to Δ. A comparison of the two, as requested in the lab brief, is shown in Figure 2.5.

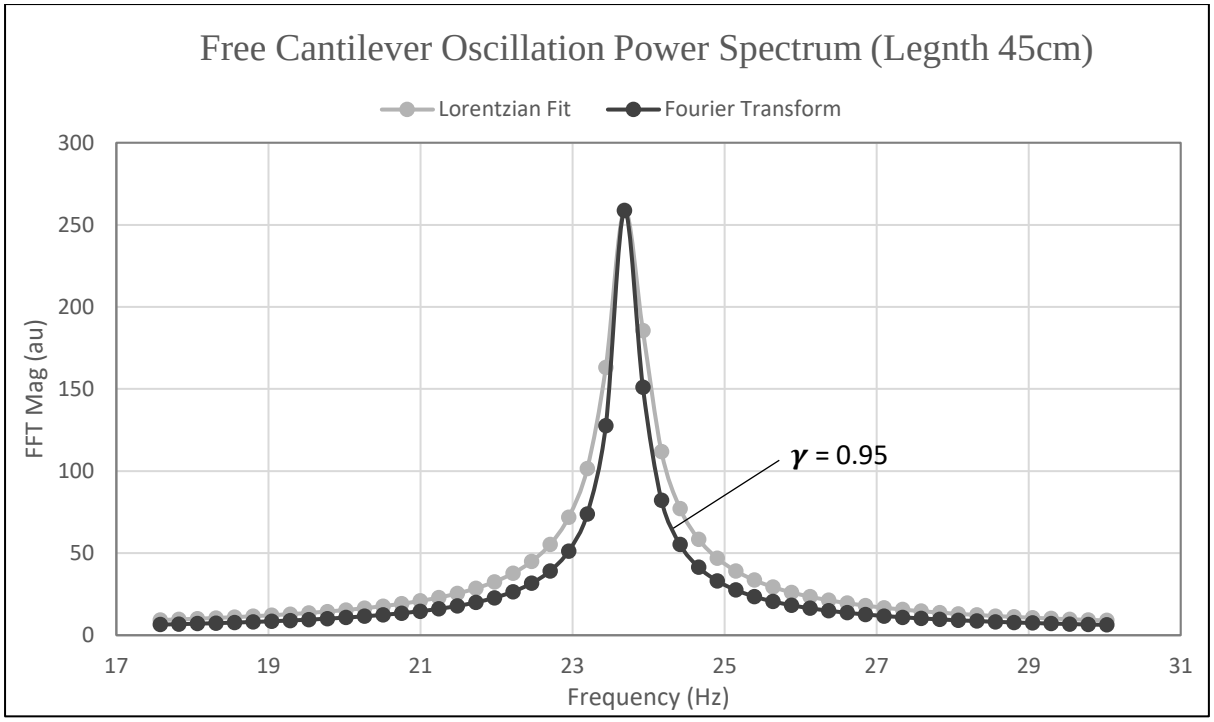

Fig 2.5 – Comparison between Fitted Lorentzian and Damped Oscillator FT at γ = 0.95

At the same arbitrary amplitude, this is evidently a very good fit. However, it is not quite perfect. **An ideal decay factor of γ =*1.37* can be solved for mathematically**, which should in theory correspond to a perfect fit.

As such, **an optimal envelope fit that corresponds to a perfect fit Lorentzian can only be found by altering the amplitude of the exponential and adding a centre off-set**. This, really, should have been done initially. The centre offsets do not violate any theory (rather, they are more rigorous) and do not change the result of the function's Fourier Transform. The updated envelopes, which align rigorously according to theory are shown below in Fig 2.6.

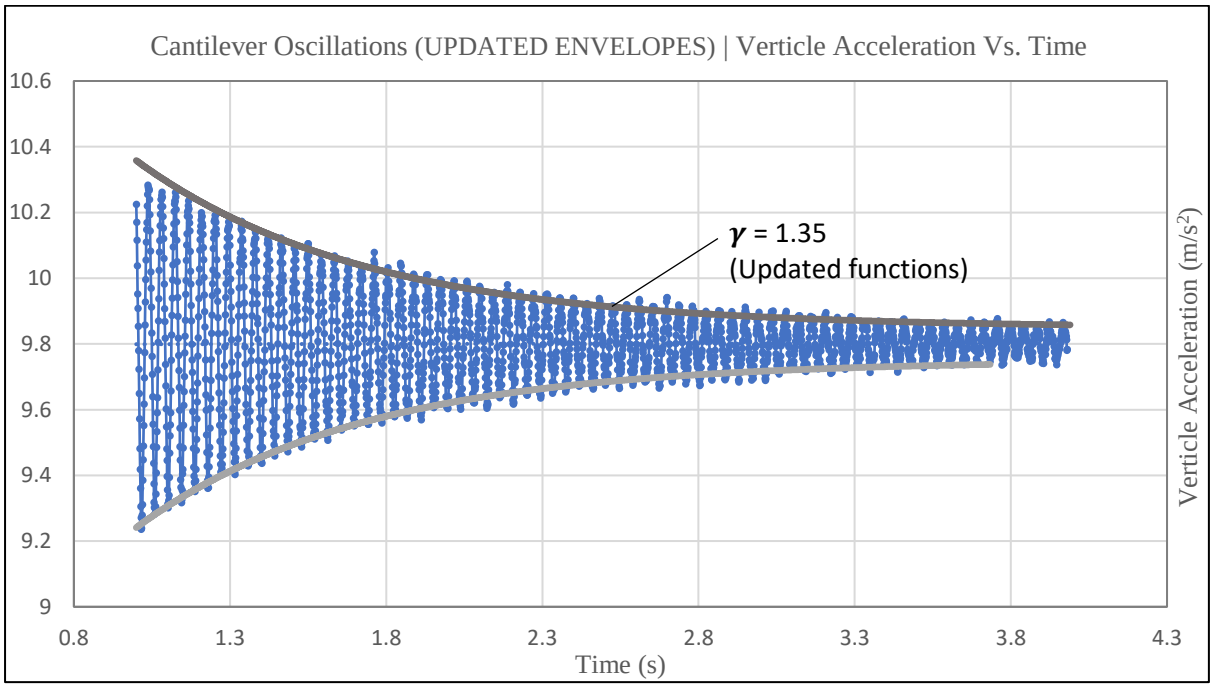

Fig 2.6 – Additionally to the update in decay factor, a centre off-set of ±0.05ms^{-2} has been applied.

3. Mass Suspended from Cantilever (b)

3.1 Theory / Procedure

As specified by the lab brief (Part 1), the spring constants had to be determined for both springs provided. A graph of T^2 Vs. m (The period of oscillation squared against effective mass) gives a straight-line slope of

$$s = \frac{4\pi^2}{k_s}$$

where k_s is the spring constant of the spring.

This was done by, firstly, setting up the experiment as shown in Figure 3.1, where the cantilever is clamped to the bench with a length of 45cm. A spring (1 of 2) and graduated mass holder was then hung from the cantilever as close as possible to the bench. For several *added masses*, from 100g to 350g, the time for 200 oscillations was recorded and documented respectively. This process was then repeated for the second spring.

Modification to Procedure: In order to obtain the best and most accurate data set (of which is shown in section 3.2), the **spring oscillations for both parts were video recorded using a smart phone** and the oscillations were counted at a slower playback speed, and timestamped accordingly (Time stamps were taken in case of an event of miscalculation or a lapse in counting occurred so that the process did not have to be completely restarted). Time stamps of oscillations were taken at 0^{th}, 50^{th}, 100^{th}, 150^{th}, and 200^{th} oscillations.

Fig 3.1 – Experimental Setup

The Young's Modulus, as specified by the lab brief (Part 2), was determined by varying the point of suspension of the mass-spring system for a constant mass along the cantilever and measuring the time for 200 oscillations of the mass spring system in vertical motion. By

assuming that the cantilever deflects significantly enough in oscillation, the period of oscillation should satisfy the following relation:

$$T^2 = 4\pi^2 m\left(\frac{1}{k_s}+\frac{1}{k_c}\right) = T_0^2\left(1+\frac{k_s x^3}{3EI}\right)$$

where T_0 is the period when the mass is suspended at the clamped end of the cantilever and k_c is the spring constant of the cantilever Similarly to the first part, the data was acquired by using a smart phone and counting the oscillations accurately at a slower play back speed. By plotting T^2 *Vs.* x^3, the value of *EI* can be obtained from the slope.

$$s = \frac{T_0^2 k_s}{3EI}$$

3.2 Experimental Data

Spring A	Video Time Stamp					Result		Spring A Data		
Added Mass	0	50	100	150	200	t_{200}		T	T^2	M
g	s	s	s	s	s	s		s	s^2	kg
100	3	29	55	81	106	103	±0.5	0.515	0.26523	0.1
150	14	43	73	102	132	118	±0.5	0.59	0.3481	0.15
200	28	60	94	127	160	132	±0.5	0.66	0.4356	0.2
250	9	45	81	116	152	143	±0.5	0.715	0.51123	0.25
300	7	45	84	122	162	155	±0.5	0.775	0.60063	0.3
350	2	43	85	126	168	166	±0.5	0.83	0.6889	0.35

Tab 3.1 – Spring A data

Spring B	Video Time Stamp					Result		Spring B Data		
Added Mass	0	50	100	150	200	Total		T	T^2	M
g	s	s	s	s	s	s		s	s^2	kg
100	2	35	60	85	111	109	±0.5	0.545	0.29703	0.1
200	3	37	70	103	136	133	±0.5	0.665	0.44223	0.2
300	13	48	88	129	171	158	±0.5	0.79	0.6241	0.3
350	8	51	92	134	176	168	±0.5	0.84	0.7056	0.35

Tab 3.2 – Spring B data

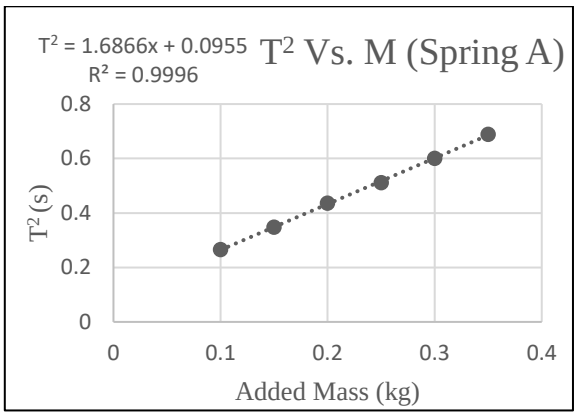

Fig 3.1 – Spring A | s = 1.6866

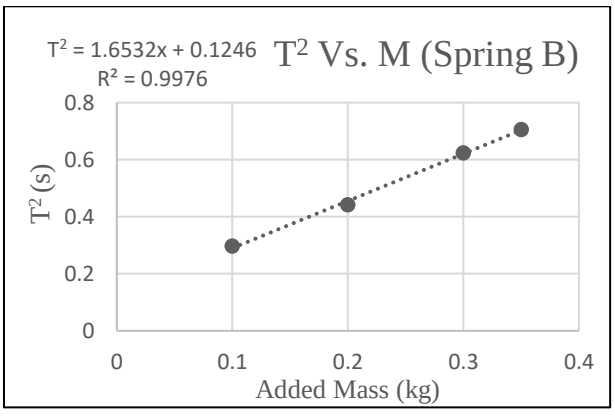

Fig 3.2 – Spring B | s = 1.6532

VARYING POINT OF SUSPENSION AND YOUNG MODULUS OF WOOD

Part 2	Video Time Stamp					Result		Data			notes
x m	0 s	50 s	100 s	150 s	200 s	t_{200} s		T s	T^2 s^2	x^3 m^3	
0.05	**48**	**87**	**129**	**170**	**231**	**183**	**±0.5**	**0.915**	**0.83723**	**0.000125**	***Outlier***
0.125	25	67	108	150	192	167	±0.5	0.835	0.69723	0.001953	
0.2	28	70	111	153	195	167	±0.5	0.835	0.69723	0.008	
0.275	10	53	95	137	178	168	±0.5	0.84	0.7056	0.020797	
0.35	18	61	103	145	188	170	±0.5	0.85	0.7225	0.042875	
0.4	21	64	107	150	192	171	±0.5	0.855	0.73103	0.064	
0.05	**2**	**43**	**85**	**126**	**168**	**166**	**±0.5**	**0.83**	**0.6889**	**0.000125**	***from Previous Section***

±0.0005

Tab 3.3 – Varying Point of suspension (Part 2) – Spring A

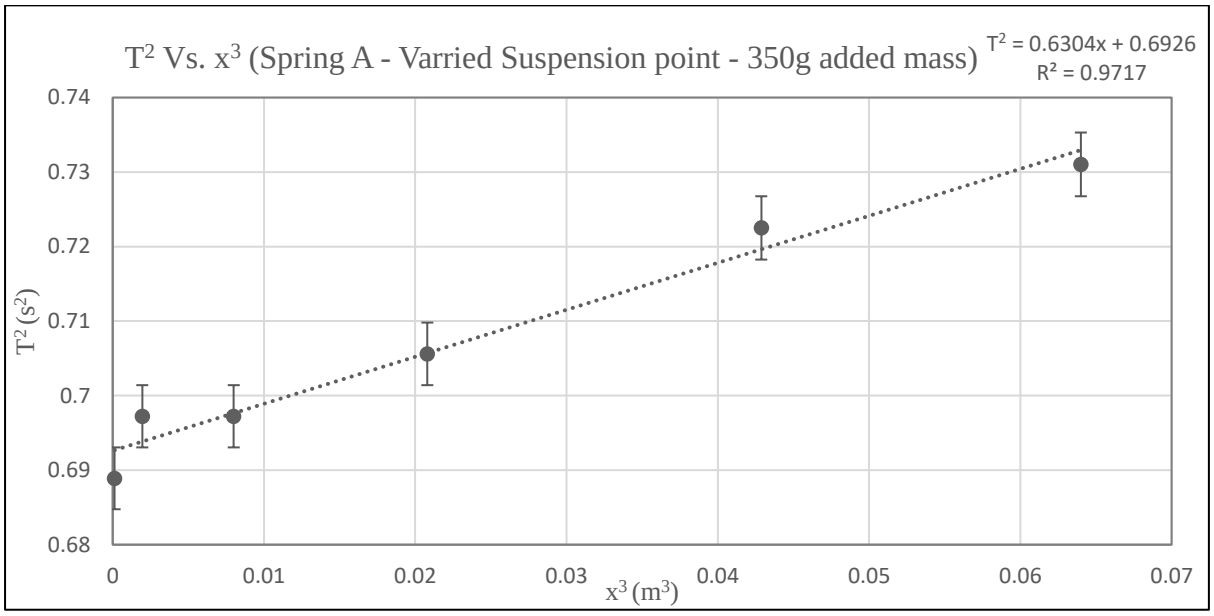

Fig 3.3 – Varied Suspension point plot (Inc. Error Bars for both axes) – s = 0.6304

3.3 Calculation / Error Analysis

Spring Constant k_s of Spring A:

$$s = 1.686614\ s^2 kg^{-1}\ \textit{(Fig 3.1)},\quad \Delta s = 0.01763$$

$$k_s = \frac{4\pi^2}{s} = \frac{4\pi^2}{1.686614} Nm^{-1} = 23.4069\ Nm^{-1}$$

$$\frac{\Delta k_s}{k_s} = \frac{\Delta s}{s} = \frac{0.01763}{1.686614} = 0.010453$$

$$\rightarrow \Delta k_s = 0.2447$$

$$\therefore \boldsymbol{k_s = 23.4 \pm 0.2\ Nm^{-1}}$$

Spring Constant k_s of Spring B:

$$s = 1.653203\ s^2\ kg^{-1}\ \textit{(Fig 3.2)},\ \ \Delta s = 0.05682$$

$$k_s = \frac{4\pi^2}{s} = \frac{4\pi^2}{1.653203} Nm^{-1} = 23.8799\ Nm^{-1}$$

$$\frac{\Delta k_s}{k_s} = \frac{\Delta s}{s} = \frac{0.05682}{1.653203} = 0.03437$$

$$\rightarrow \Delta k_s = 0.8207$$

$$\therefore \boldsymbol{k_s = 23.9 \pm 0.8\ Nm^{-1}}$$

Young's Modulus of Cantilever, *E*:

$$s = 0.630357\ s^2\ m^{-3}\ \textit{(Fig 3.3)},\ \Delta s = 0.053825,$$

$$T_0 = 0.83,\ \Delta T_0 = 0.005\ s\ \textit{(Table 3.3 – result for 0.05m)},$$

$$I = 7.1197 \times 10^{-10}\ m^4,\ \frac{\Delta I}{I} = 0.1739548\ \textit{(Section 2.3)},\ \Delta T_0 = 0.005\ s$$

$$s = \frac{k_s T_0^2}{3EI} \rightarrow E = \frac{k_s T_0^2}{3Is} = \frac{(23.4069\ Nm^{-1})(0.6889\ s^2)}{3(7.12 \times 10^{-10}\ m^4)(0.630357\ s^2 m^{-3})} = 1.198 \times 10^{10} Nm^{-2}$$

$$\frac{\Delta E}{E} = \frac{\Delta k_s}{k_s} + \frac{\Delta I}{I} + \frac{\Delta s}{s} + 2\frac{\Delta T_0}{T_0} = 0.03437 + 0.1739548 + \frac{0.053825}{0.630357} + 2\frac{0.005}{0.83} = 0.3057$$

$$\rightarrow \Delta E = 0.36628 \times 10^{10} Nm^{-2}$$

$$\therefore\ \boldsymbol{E = (1.2 \pm 0.4) \times 10^{10}\ Nm^{-2}}$$

Specified factor *EI*:

$$E = \frac{k_s T_0^2}{3Is} \rightarrow EI = \frac{k_s T_0^2}{3s} = \frac{(23.4069\ Nm^{-1})(0.6889\ s^2)}{3(0.630357\ s^2 m^{-3})} = 8.5269 Nm^2$$

$$\frac{\Delta EI}{EI} = \frac{\Delta k_s}{k_s} + \frac{\Delta s}{s} + 2\frac{\Delta T_0}{T_0} = 0.1318$$

$$\rightarrow \Delta EI = 1.1239\ Nm^2$$

$$\therefore \boldsymbol{EI = (8.5 \pm 1.1) \times 10^{10} Nm^2}$$

3.4 Results / Discussion

Based on the data collected (as shown in section 3.2) and the analysis in section 3.3, the results for Experiment (b) are as follows:

$$\boldsymbol{k_s(A) = 23.4 \pm 0.2\ Nm^{-1}}$$
$$\boldsymbol{k_s(B) = 23.9 \pm 0.8\ Nm^{-1}}$$
$$\boldsymbol{E = (1.2 \pm 0.4) \times 10^{10}\ Nm^{-2}}$$
$$\boldsymbol{EI = (8.5 \pm 1.1) \times 10^{10} Nm^2}$$

These results are, in my opinion, a plausible representation of reality given that the values presented above seem to be typical in terms common source information. I know from my previous studies in PY1052 that the spring constant of the department provided springs should

in fact be in the range of *23 – 25 N/m*, so there is nothing extraordinary to discuss in terms of these particular results.

In the analysis of section 2.1 (Experiment a) we determined (via respective alternative method) the value of E and EI to be

$$E = (1.0 \pm 0.1) \times 10^{10}\ Nm^{-2}$$

$$EI = 7.2 \pm 0.2\ Nm^{2}$$

By a (not so rigorous) qualitative analysis of the combined results, the produced answer for both the Young's Modulus of the cantilever, *E*, and factor *EI* are within the appropriate margins of error determined. Particularly interesting to note is that the upper limit of *EI* from *Experiment a* seems to be (approximately, of course) the lower limit of error determined in *Experiment b*.

Comparing the two values of *E* determined via the two methods documented; they are within reasonable margins of error with respect to each other, and both seem like an accurate reflection of reality. The typical Young's Modulus of Fir is

$$^{[2]}\ E_{fir} = (9.7\ to\ 13.4) \times 10^{10}\ Nm^{-2}\,.$$

(Aside: "White deal" is a type of Fir, and would be a strong contender to be the exact material of the half meter stick used in this experiment due to its availability and cheap price – making it a popular choice for common wooden commercial products such as our half meter stick – regardless, our experimentally determined E is within the same order of magnitude of most wood types listed in Reference [2])

4. Moments of Inertia and Torsional Oscillation (c)

4.1 Angle of Inclination of Earth's Magnetic Field *(Exercise)*

As an exercise, the lab brief specifies to determine the magnitude and angle of inclination of the earths magnetic field to the horizontal. This was done using the phyphox Magnetic Spectrum and exporting the raw sensor data. Each directional component of the field was then estimated (with appropriate error). The Compiled data is shown in Table 4.1. A visualisation of the data is shown in vector form in Figure 4.1.

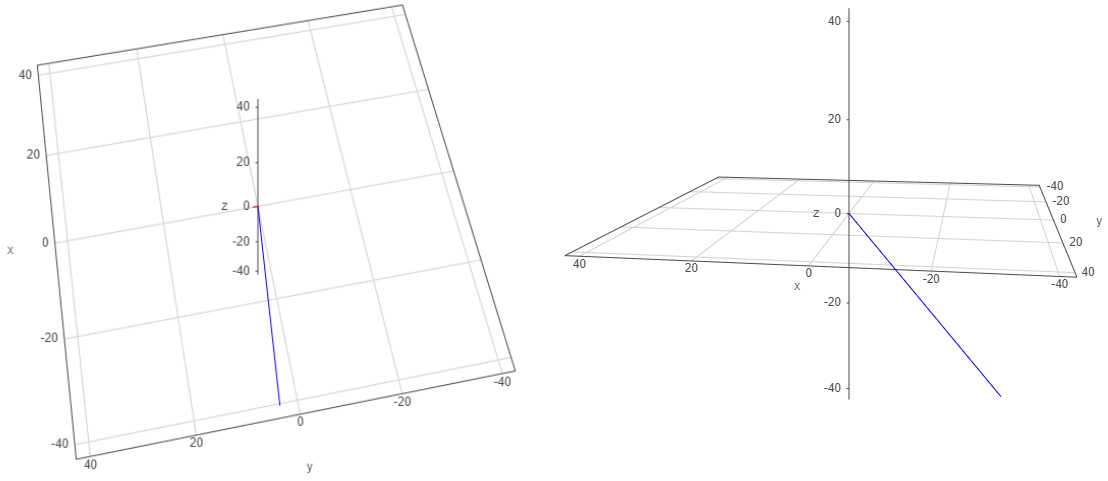

Fig 4.1 – Earths Magnetic Field Vector (BLUE) and B_y contribution (RED) – Plotted in units of µT

	Avg. Mag T	Max T	Min T
$\mathbf{B_x}$	-3.34E-05	-3.24E-05	-3.44E-05
$\mathbf{B_y}$	1.02E-07	1.22E-06	-1.16E-06
$\mathbf{B_z}$	-3.89E-05	-3.78E-05	-3.99E-05

	B T		
$\mathbf{B_x}$	-3.34E-05	±	1.01E-06
$\mathbf{B_y}$	1.02E-07	±	1.12E-06
$\mathbf{B_z}$	-3.89E-05	±	1.02E-06

$$|B| = (5.13 \pm 0.18) \times 10^{-5}\ T$$

Tab 4.1 – Collected Data

As is evident in the displayed data and visualised in Figure 4.1, the y component, for the purpose of this exercise, is negligible (this is a coincidence). This simplifies the calculation the angle of inclination to a 2-dimensional problem. Simple trigonometry shows:

$$\tan\theta = \frac{B_z}{B_x} \quad \rightarrow \quad \theta = \tan^{-1}\frac{-3.89}{-3.34} = 49.35°$$

To verify, explicitly, by elementary vector analysis of all components:

$$\bar{B} \cdot \bar{h} = |B||h| \cos\theta$$

where $\bar{h}$ is an appropriate 'horizontal' vector.

$$\bar{h} = \begin{pmatrix} -1 \\ 1.02 \times 10^{-7} \\ 0 \end{pmatrix}, \quad |B| = 5.127 \times 10^{-5}, \quad |h| \cong 1$$

$$\begin{pmatrix} -3.34 \times 10^{-5} \\ 1.02 \times 10^{-7} \\ -3.89 \times 10^{-5} \end{pmatrix} \cdot \begin{pmatrix} -1 \\ 1.02 \times 10^{-7} \\ 0 \end{pmatrix} = (5.127 \times 10^{-5}) \cos\theta$$

$$\theta = \cos^{-1}\left(\frac{3.34 \times 10^{-5} + 1.0404 \times 10^{-15}}{5.127 \times 10^{-5}}\right) = 49.348°$$

As such, The earths magnetic field is $5.127 \times 10^{-5}\ T$ in magnitude at $-49.35°$ to the horizontal (into the ground). Since the angle of inclination is not a value that will be used experimentally, an error analysis is of no concern.

Note: This measurement had to be taken many times. My area of residence, being a dense accommodation block, seems to have a noticeably variated magnetic field, in fact **the measurement above was conducted outside in the car park**, as it was very difficult to obtain consistent results from inside. For example, shown below are two additional results showcasing this variation just meters apart (for these two measurements, it was ensured that the phone was kept at a consistent angle to the horizontal).

	Avg. Mag μT
$\mathbf{B_x}$	-21.10319909
$\mathbf{B_y}$	-17.37722243
$\mathbf{B_z}$	-47.65869299

$\theta = 59.93°$

	Avg. Mag μT
$\mathbf{B_x}$	-0.4262
$\mathbf{B_y}$	10.30071
$\mathbf{B_z}$	-37.9009

$\theta = 83.05°$

Tab 4.2 – Kitchen Measurement | Hallway Measurement

(See submitted data sheets for calculation – stored under 'Additional Magnetic Spectrum')

4.2 Theory / Procedure *(Experiment)*

If the radius of gyration about an axis is R, the moment of inertia is as such

$$I = MR^2$$

where *M* is the mass of the body. The ratio of the period of torsional oscillation T_l to the period of vertical oscillation T_v is therefore

$$\frac{T_l}{T_v} = R\sqrt{\frac{k}{C}}$$

where *k* is the spring constant of the system and C is the restoring constant for torsion. As mentioned on the overview page (*section 1*), the goal of *Experiment c* is to determine the Principal Moments of Inertia of a uniform and potentially non-uniform mass distribution (i.e. phone and MDF block). The gyration radius of a uniform rectangular block about an axis through it's centre of mass perpendicular to a side of length *L* is

$$R_b = \frac{L}{\sqrt{12}}$$

By following the procedure/method as detailed in the lab manual, where the torsional oscillation period of the uniform block (in horizontal and vertical orientation) along with the vertical oscillation period of the block are determined; the value of $\sqrt{k/C}$ can be determined by recognising that

$$\sqrt{\frac{k}{C}} = \frac{\sqrt{12}}{L}\frac{T_{bl}}{T_{bv}}$$

From $\sqrt{k/C}$, the gyration radius and principle moment of inertia can be determined for the orientations of the smart phone under the same conditions.

Modifications to Setup: There were a number of issues with experimental setup, mainly the issue encountered was that the value of $\sqrt{k/C}$ was not consistent among the two orientations of the uniform block. Several modifications were a necessary requirement, as the initial attempts of getting coherent results was likely ***impossible*** with the setup recommended. The zip lock bag setup, shown in Figure 4.1, was swapped out for a much more elegant and purpose-built setup which made use of **additional picture hooks, string, and safety pins** (See Figure 4.2 for updated setup). This came with many advantages, including the ability to **set the block *far* more confidently in torsional oscillation about the exact centre of the axis**, rather than just approximately according to eye. More details regarding the change in setup will be discussed in section 4.5. The data for each respective setup is shown in Section 4.3.

Fig 4.1 – Initial Setup

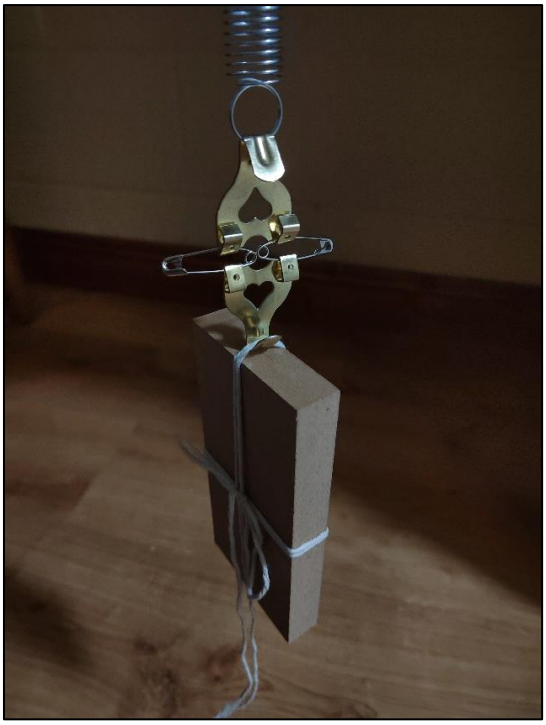

Fig 4.2 – Updated Setup

Unfortunately, a solution could not be reach for the phone. However, the issues encountered for the block did not necessarily apply to the phone due to its increased mass, so the setup as seen in Fig 4.1 was used to collect data for the phone (in the procedure specified as per the lab manual).

4.3 Experimental Data

Using setup as shown in Figure 4.1:

MDF block (vertical orientation)	t s	#Osc N	T s
Torsional Oscillation	68.64	20	3.43
Vertical Oscillation	25.5	50	0.51

L (Block width) m	T_{bs} T_{bv}	R_b m	$\sqrt{(k/C)}$
0.0712	6.729412	0.020554	327.4068
±0.0005			

MDF block (horizontal orientation)	t s	#Osc N	T s
Torsional Oscillation	94.98	20	4.75
Vertical Oscillation	25.5	50	0.51

L (Block length) m	T_{bl} T_{bv}	R_b m	$\sqrt{(k/C)}$
0.15	9.311765	0.043301	215.046
±0.0005			

Tab 4.2 – Initial Data for Torsional Oscillation of MDF Block

Using setup as shown in Figure 4.2 (improved setup):

MDF block (vertical orientation)	t s	#Osc N	T s
Torsional Oscillation	39.46	20	1.97
Vertical Oscillation	23.78	50	0.48

L (Block Width) m	T_{bs} T_{bv}	R_b m	$\sqrt{(k/C)}$
0.072	4.148444	0.020785	199.5921
±0.0005			

MDF block (horizontal orientation)	t s	#Osc N	T s
Torsional Oscillation	81.56	20	4.08
Vertical Oscillation	23.78	50	0.48

L (Block length) m	T_{bl} T_{bv}	R_b m	$\sqrt{(k/C)}$
0.15	8.574432	0.043301	198.018
±0.0005			

Tab 4.3 – Updated/Improved Data for Torsional Oscillation of MDF Block

**The string length (cantilever to spring) did not change between the recording of two block data sets.*

Phone Oscillation Data:

$\underline{T_{pl}}$ s	$\underline{T_{ps}}$ s	$\underline{T_{pv}}$ s	$\underline{\frac{T_{pl}}{T_{pv}}}$	$\underline{\frac{T_{ps}}{T_{pv}}}$	$\underline{M_{phone}}$ kg
5.6132	3.2872	0.65	8.6346	5.05723	0.213
±0.0005	±0.0005	±0.005			±0.0005

Tab 4.4 – Phone Oscillation data

4.4 Calculation / Error Analysis

$$\sqrt{\frac{k}{C}} = \frac{\sqrt{12}}{L}\frac{T_{torsional}}{T_{vertical}}, \qquad R = \frac{T_{torsional}}{T_{vertical}}\sqrt{\frac{C}{k}}$$

Using data from Table 4.3:

$$\Delta T_b \approx 0.005$$

Principle Moment of Inertia of Phone and Gyration Radius perpendicular to *long* side of phone from combined data of Table 4.4 and calculation above:

Taking $\sqrt{k/C}$ *= 199.5921*

$$R_{pl} = \frac{T_{pl}}{T_{pv}}\sqrt{\frac{C}{k}} = (8.6346)(199.5921)^{-1} = 0.04326\ m$$

$$\rightarrow \Delta R_{pl} = (0.0285)(0.02168\ m) = 6.17 \times 10^{-4}\ m$$

$$\therefore \boldsymbol{R_{pl} = (4.33 \pm 0.06) \times 10^{-2}\ m}$$

$$I_{pl} = MR^2 = M\left(\frac{T_{pl}}{T_{pv}}\sqrt{\frac{C}{k}}\right)^2 = (0.213\ kg)(0.04326\ m)^2 = 3.98 \times 10^{-4}\ kg\ m^2$$

$$\frac{\Delta I_{pl}}{I_{pl}} = 2\frac{\Delta R_{pl}}{R_{pl}} + \frac{\Delta M}{M} = 2(0.0285) + \frac{\Delta M}{M} = 2(0.0285) + \frac{0.0005}{0.213} = 0.0593$$

$$\rightarrow \Delta I_{pl} = (0.0593)(3.98 \times 10^{-4}\ kg\ m^2) = 0.36 \times 10^{-6}\ kg\ m^2$$

$$\therefore \boldsymbol{I_{pl} = (3.98 \pm 0.04) \times 10^{-4}\ kg\ m^2}$$

Principle Moment of Inertia of Phone and Gyration Radius perpendicular to *short* side of phone from combined data of Table 4.4 and calculation above:

$$R_{ps} = \frac{T_{ps}}{T_{pv}}\sqrt{\frac{C}{k}} = (5.05723)(199.5921)^{-1} = 0.02534\ m$$

$$\rightarrow \Delta R_{ps} = (0.0291)(0.02534\ m) = 7.38 \times 10^{-4}\ m$$

$$\therefore \boldsymbol{R_{ps} = (2.53 \pm 0.07) \times 10^{-2}\ m}$$

$$I_{ps} = MR^2 = M\left(\frac{T_{ps}}{T_{pv}}\sqrt{\frac{C}{k}}\right)^2 = (0.213\ kg)(0.02534\ m)^2 = 1.37 \times 10^{-4} kg\ m^2$$

$$\rightarrow \Delta I_{ps} = (0.0611)(1.37 \times 10^{-4}\ kg\ m^2) = 8.3 \times 10^{-6}\ kg\ m^2$$

$$\therefore \boldsymbol{I_{ps} = (1.37 \pm\ 0.08) \times 10^{-4}\ kg\ m^2}$$

4.5 Results / Discussion

Based on the data collected (as shown in section 4.3) and the analysis in section 4.4, the results for *Experiment (c)* are as follows:

$$R_{bl} = (4.33 \pm 0.01\ ) \times 10^{-2}\ m,\ \ R_{bs} = (2.08 \pm 0.01\ ) \times 10^{-2}\ m$$

$$R_{pl} = (4.33 \pm 0.06) \times 10^{-2}\ m,\ \ R_{ps} = (2.53 \pm 0.07) \times 10^{-2}\ m$$

$$I_{pl} = (3.98 \pm 0.04) \times 10^{-4}\ kg\ m^2$$

$$I_{ps} = (1.37 \pm\ 0.08) \times 10^{-4}\ kg\ m^2$$

The difference and consistency of the produced value of $\sqrt{(k/C)}$ between the two data sets shown in Tables 4.2 and 4.3 is staggering. I do not believe it would have been possible to produce answers to the confidence present in the above without redesigning the experiment apparatus. The design in Figure 4.2 is clearly superior in the quality of its produced data. I would like to claim this because the updated design can be confidently centred with the rotation axis and the design does not encounter significant air resistance imposed on the system by the zip lock bag (This was particularly prominent and noticeable for the block due to its lower mass).

Interpreting the Gyration Radius results; it seems to me that **the phone has a very uniform mass distribution**. The values R_{bl} and R_{pl} computed are strikingly similar, at least in comparison to R_{bl} and R_{pl}, where the two are not so obviously comparable. This discrepancy could be due to the setup, for the reasons discussed previous. However, it seems reasonable to assume that densely packed electronics would not necessarily be uniformly distributed in all axes, especially considering the size of batteries in modern mobile phones, which are (assumedly) of differing density to other components. This is a plausible explanation for the case of the smartphone used, the *Honor 50*. I have claimed this judging by the image of a teardown of the phone shown in Figure 4.3. The battery seems to be the same width as the phone, but it is off centred about the axis perpendicular to the side length of the device. Therefore, it is reasonable to conclude that the results achieved could be a good reflection of reality.

Fig 4.3 [3] – Honor 50 Teardown, See Reference [3] for Source.

The raw sensor data was exported with FFT power spectrums, from which we can verify the periods of oscillation settled for:

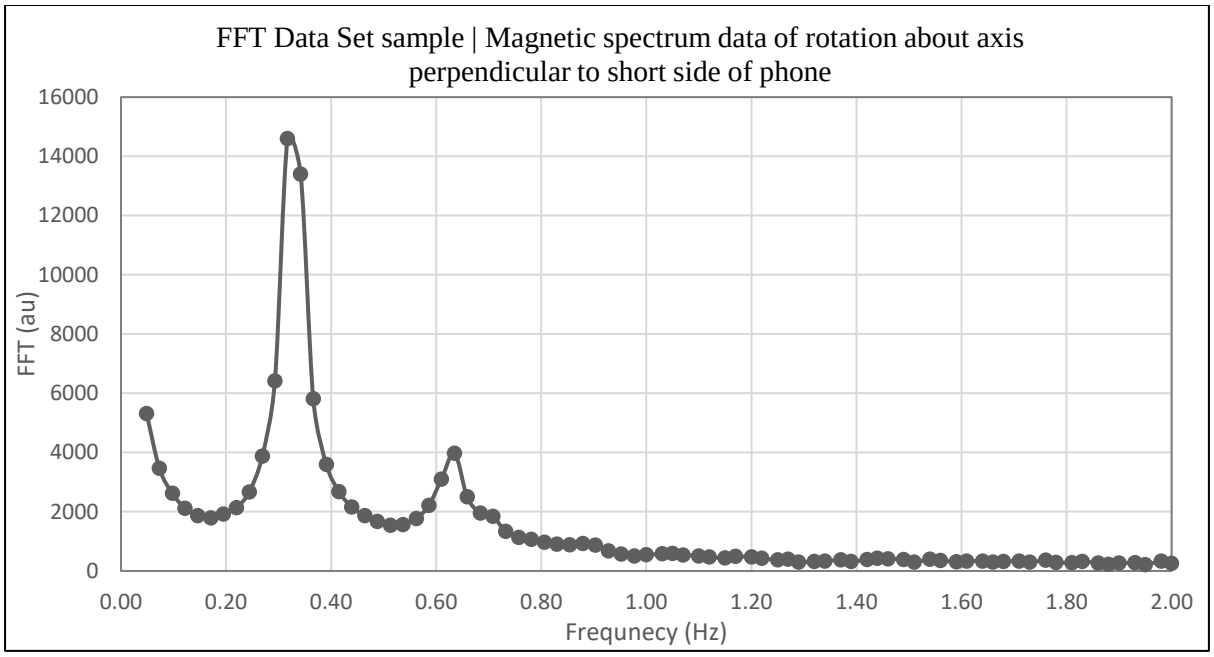

Fig 4.4 – Frequency peak at 0.317 Hz

$$f_{peak} = 0.317\ s^{-1} \ \rightarrow \ T_{ps} = \frac{1}{0.317} = 3.155\ s \ \approx 3.28\boldsymbol{s} = T_{ps\ Ex}$$

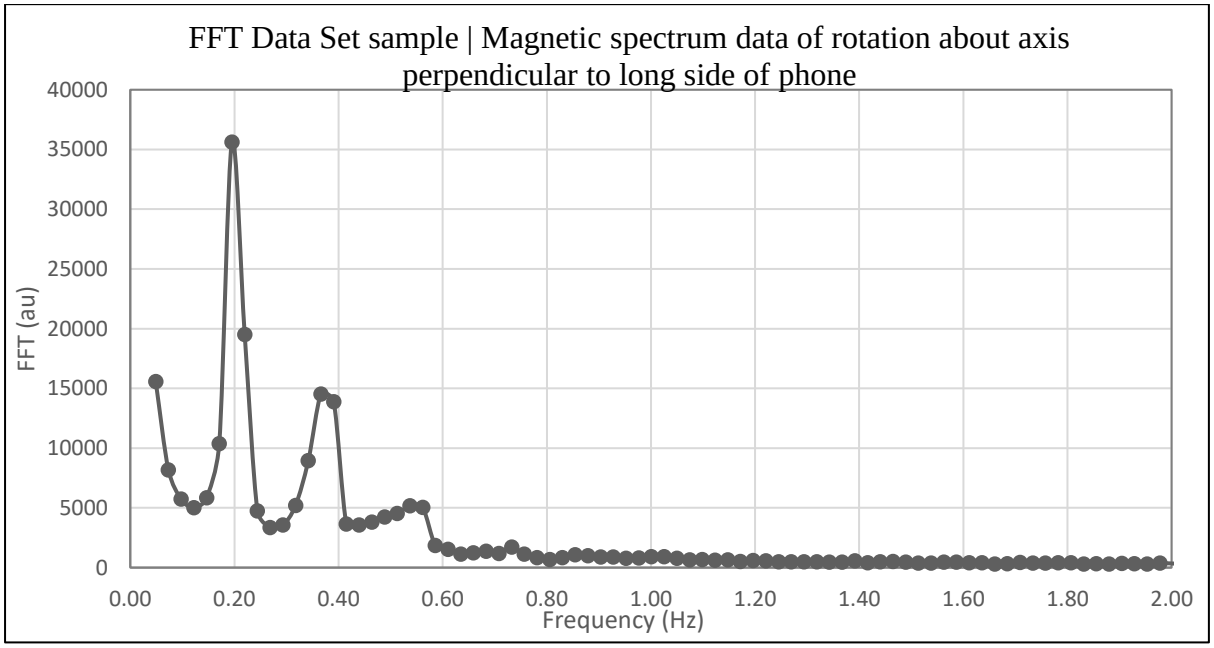

Fig 4.5 – Frequency peak at 0.195 Hz

$$f_{peak} = 0.195\ s^{-1} \ \rightarrow \ T_{ps} = \frac{1}{0.195} = 5.128\ s \approx 5.61\ \boldsymbol{s} = T_{ps\ Ex}$$

FFT observations: Taking a look at the FFTs produced, there is an additional prominent peak at double the torsional oscillation frequency. This can be identified in the raw data:

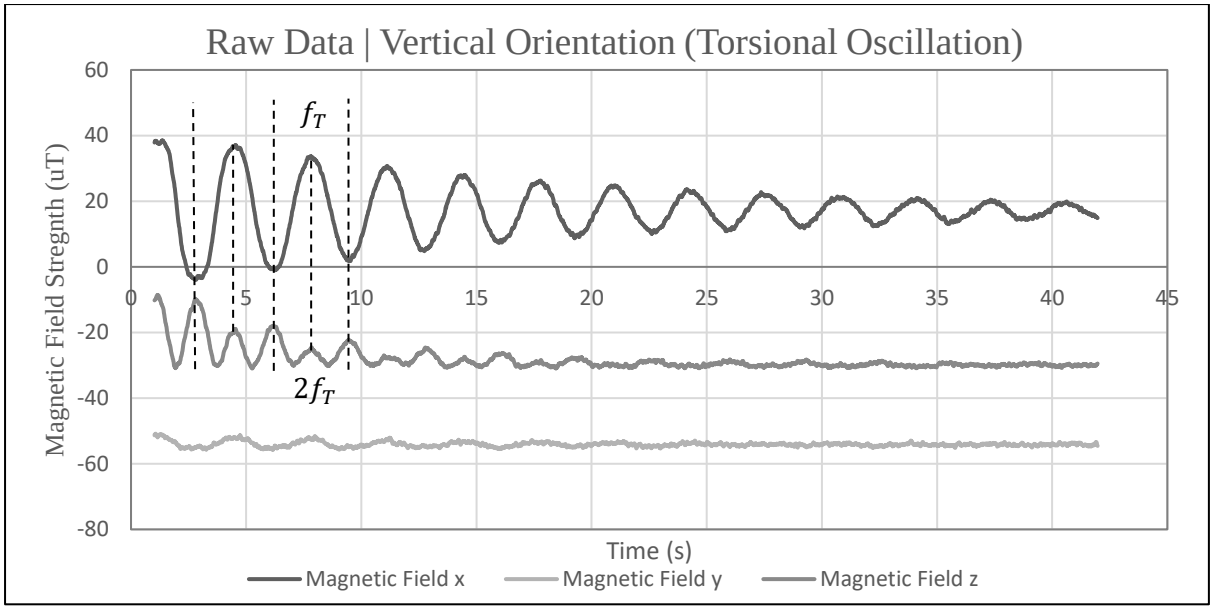

Fig 4.5 – Vertical Orientation Raw Data for Torsional Oscillation

The data recorded from the y-sensor is clearly double the frequency of the data recorded in the x. I would be led to believe that **this is possibly due to slight pendulum motion of the system while taking measurements,** I have found this very difficult to conclude however; as in a later experiment this is ultimately disproved since the torsional frequencies observed did not align with pendulum modes (See experiment *e*). In both FFT's, (For vertical and horizontal orientation of the phone) **these frequencies are consistently 2:1** even though the systems have been altered and the torsional frequency is changed due to differing moments of inertia.

5. Coupled Masses on a Cantilever (d)

5.1 Theory/Procedure

In this section we investigate the phenomenon of beats, studying the frequencies of coupled modes of vertical oscillation of our smartphone and another known mass suspended from the cantilever we have been working with throughout this report. For the setup described (and demonstrated in Fig 5.1) the periods of normal modes can be determined using the relation

$$T_{\pm}^2 = \frac{T_1^2 + T_2^2}{2} \pm \sqrt{\left(\frac{T_1^2 - T_2^2}{2}\right)^2 + K^2}$$

where T_1 is the period of $m_1$on its own, T_2 is the period of $m_2$on its own, and K is the cantilever coupling according to

$$K = 2\pi^2 \frac{\sqrt{m_1 m_2}}{3EI} x_1^2 (3x_2 - x_1).$$

where m_1 is the phone mass at a distance x_1 along the cantilever and m_2 is the graduated mass at a distance $x_2$along the cantilever according to Fig 5.1.

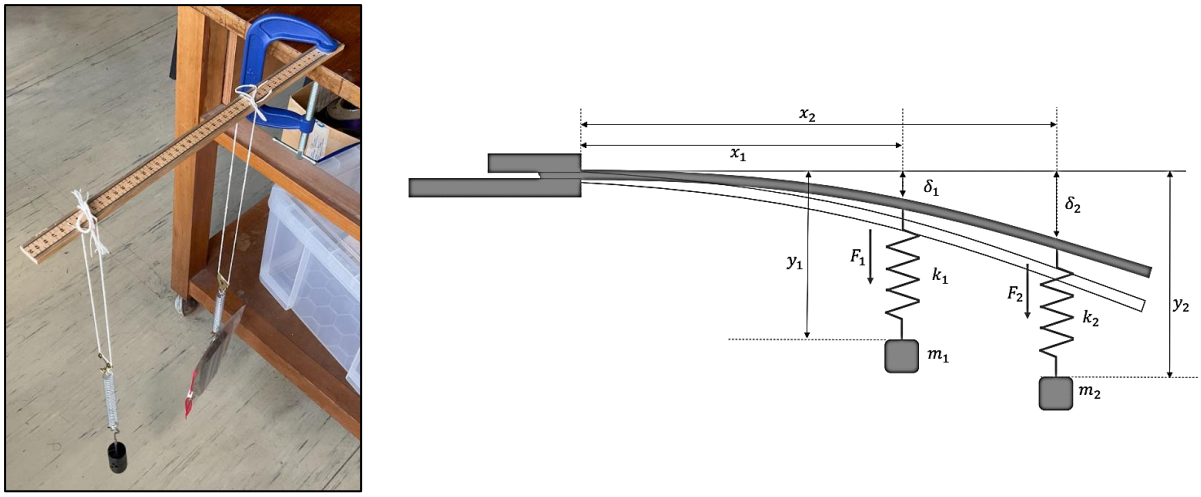

Fig 5.1 | Experimental and Schematic Setup

The experiment was setup as shown in Figure 5.1 (see also Figure 5.2), the procedure used to obtain the experimental data as shown in section 5.2 is **identical** to the provided/recommended procedure in the lab manual.

5.2 Experimental Data

The following parameters remained **constant** for the data shown in this section:

Cantilever Suspensions					
Clamped	**Phone**	**Masses**	**Phone (Corrected)**	**Masses (Corrected)**	**EI**
m	**m**	**m**	**m**	**m**	**Nm^2**
0.05	0.35	0.49	0.3	0.44	7.2
±0.001	±0.001	±0.001	±0.001	±0.001	±0.2

Tab 5.1 | Cantilever Suspension points and previously determined EI, See Fig 5.2

m	**Peak 1**	**Peak 2**	**(+) T^2**	**(-) T^2**	**splitting**
kg	**Hz**	**Hz**	**s^2**	**s^2**	**s^2**
0.1	1.5502	1.8859	0.416125696	0.28116592	0.134959776
0.15	1.538	1.6479	0.422753614	0.368246216	0.054507398
0.155	1.5381	1.6296	0.422698645	0.37656328	0.046135365
0.16	1.532	1.6174	0.426071485	0.382265516	0.043805968
0.165	1.53	1.6	0.427186125	0.390625	0.036561125
0.17	1.5198	1.593	0.432939409	0.394065531	0.038873878
0.175	1.5136	1.5807	0.436493481	0.400222125	0.036271356
0.18	1.5014	1.5747	0.443615975	0.403277828	0.040338147
0.185	1.4953	1.5686	0.447242775	0.406420475	0.0408223
0.19	1.4831	1.5686	0.454631088	0.406420475	0.048210614
0.195	1.4709	1.5625	0.462204005	0.4096	0.052604005
0.2	1.4526	1.5624	0.473923147	0.409652434	0.064270713
0.25	1.3367	1.5563	0.559670098	0.412870036	0.146800062
0.3	1.2451	1.5563	0.645047258	0.412870036	0.232177222
0.35	1.1718	1.5563	0.728270993	0.412870036	0.315400958

Tab 5.3 | Experimental Data

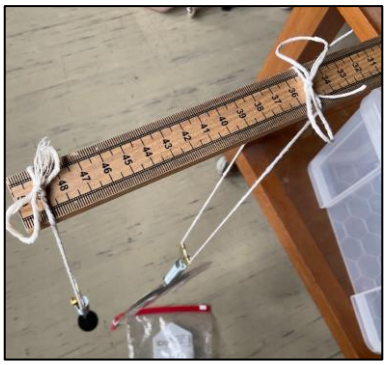

Fig 5.2 | Reference for Tab 5.1

Springs		
k_a	**k_b**	**M_{phone}**
Nm^{-1}	**Nm^{-1}**	**kg**
23.4	23.9	0.237303
±0.2	±0.8	±0.0000005

Tab 5.2 | Other useful constants

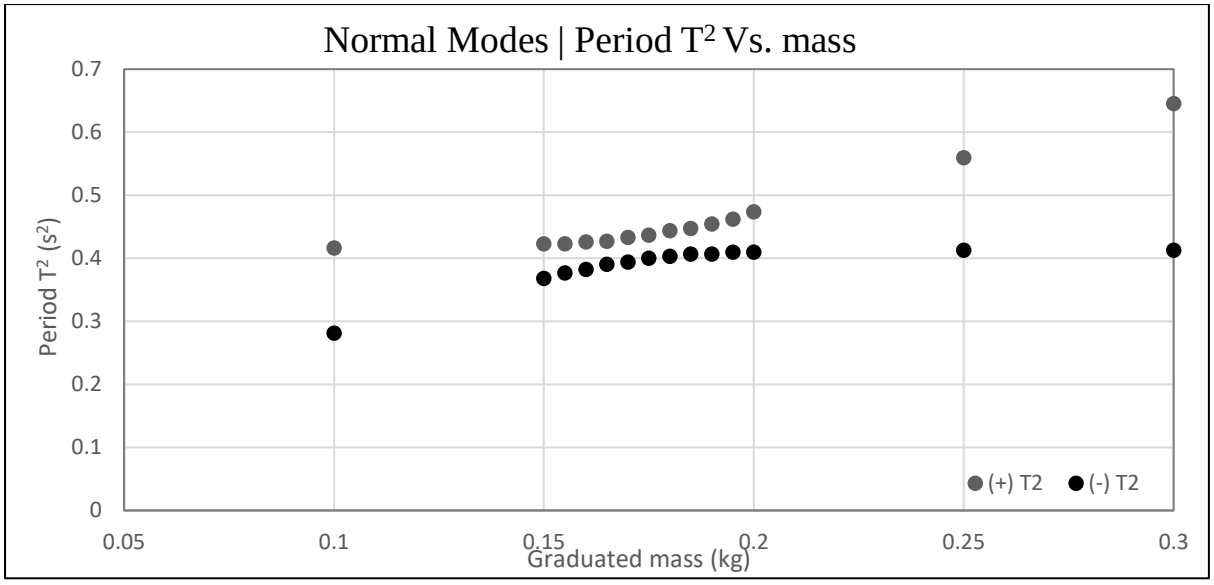

Fig 5.3 | Experimental Data, Avoided crossing observed as expected from theory

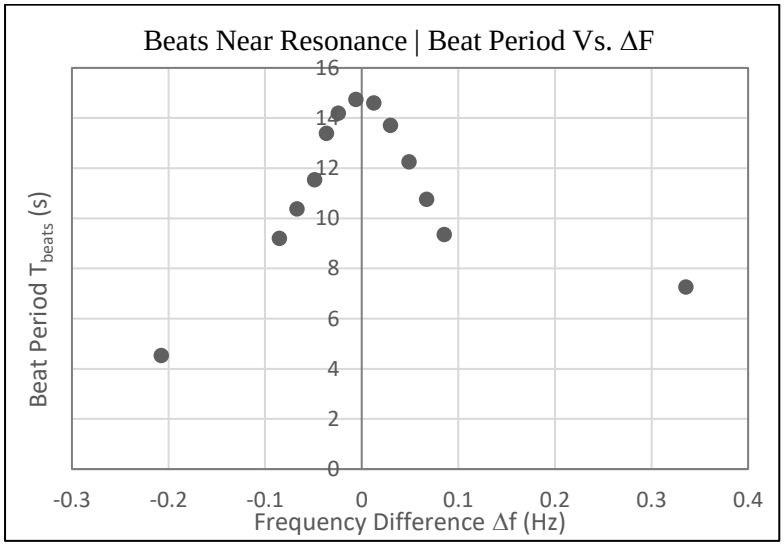

m kg	ΔF Hz	T_{Beats} s
0.1	0.3357	7.266666667
0.15	0.0855	9.361764706
0.155	0.0673	10.75928571
0.16	0.049	12.26153846
0.165	0.0296	13.71818182
0.17	0.0124	14.6
0.175	-0.0061	14.75
0.18	-0.0243	14.2
0.185	-0.0365	13.38916667
0.19	-0.0487	11.53923077
0.195	-0.067	10.376
0.2	-0.0853	9.204705882
0.25	-0.2074	4.536363636

Fig 5.4 | Beat period increases near resonance

5.3 Calculation / Error Analysis

Earlier in section 3.2 we obtained a relation for the squared period of oscillatory motion for our two provided springs as a function of mass. Particularly, the interpolation of data in Figures 3.1 and 3.2 led us to conclude:

$$T_1^2 = (1.6866m + 0.0955)\ s^2$$

$$T_2^2 = (1.6532m + 0.1246)\ s^2$$

where T_1^2 utilises the spring constant of spring *A* (k_a), T_2^2 utilises the spring constant of spring B (k_b) and *m* represents the mass attached to the springs. Calculating the theoretical cantilever coupling *K* from

$$K = 2\pi^2 \frac{\sqrt{m_1 m_2}}{3EI} x_1^2 (3x_2 - x_1)$$

And then utilising the above equations to get a theoretical value for the normal modes of vibration using

$$T_{\pm}^2 = \frac{T_1^2 + T_2^2}{2} \pm \sqrt{\left(\frac{T_1^2 - T_2^2}{2}\right)^2 + K^2}$$

we can make a good approximation of *relative error* (comparison to theoretically calculated values) in a tabular format, from which we get the following means:

Mean Relative Error T_+ = 2.8%

Mean Relative Error T_- = 2.7%

Please see the submitted spreadsheets for tables and calculations.

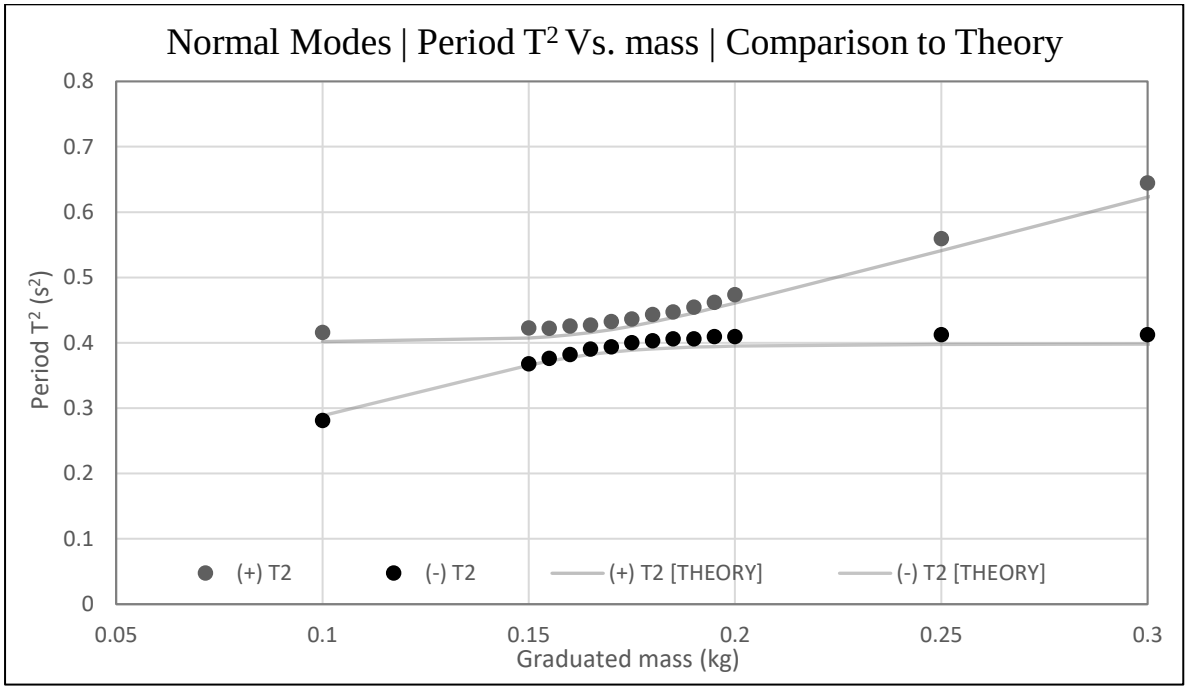

Fig 5.4 | Beat period increases near resonance

We should expect the **cleanest production of beats (resonance) at around 170g of added mass**, as per Figure 5.3. However, **this was not actually observed to be the case**. The cleanest production of beats was observed at **185g**. The raw data for this run (185g added mass) shows:

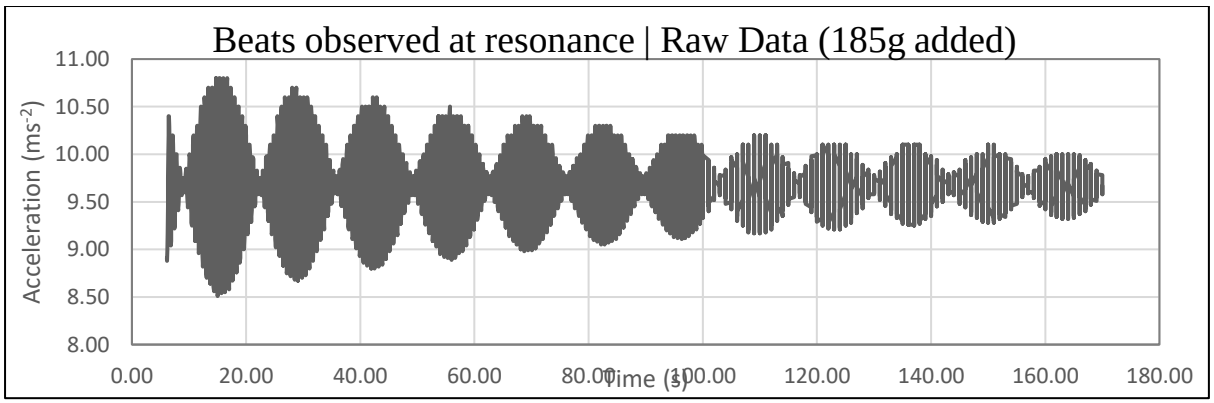

Fig 5.5 | Beats from Raw Data | 185g added mass

Which is qualitatively is in stark comparison to the data where we would have expected resonance (170g added mass) in Figure 5.6:

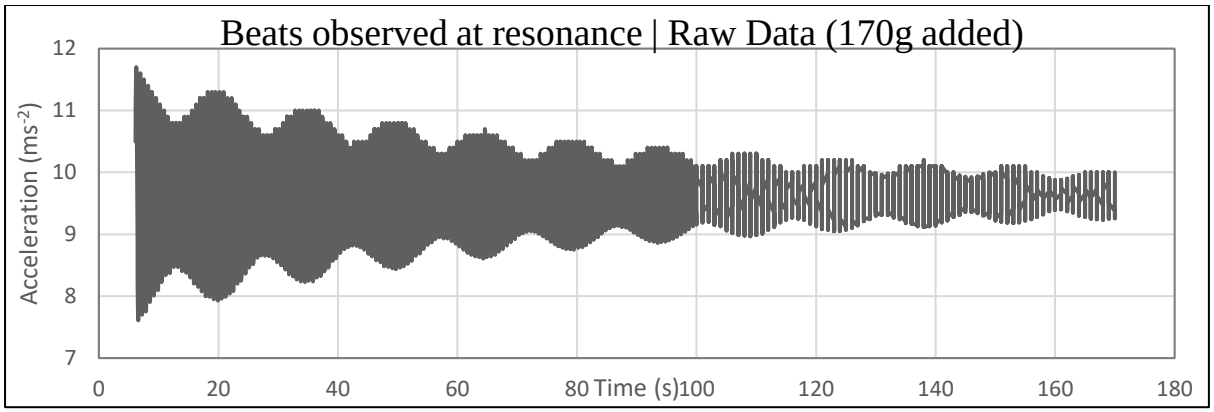

Fig 5.6 | Beats from Raw Data | 170g added mass

5.4 Further Investigation

5.4.1 Reducing K (cantilever coupling) experimentally

We know, as already stated, that

$$K = 2\pi^2 \frac{\sqrt{m_1 m_2}}{3EI} x_1^2 (3x_2 - x_1)$$

The dependence here on cantilever suspension points gives us an opportunity to review the effects of reducing *K* by altering the position of the phone on the cantilever.

A number of additional measurements were taken using an identical procedure to the previous section. From the combined figures in Figure 5.6 (next page) we can see that the beat period increases as the phone suspension point x_1 approaches *0m*. This means that theoretically **as *K* approaches 0; the observed avoided crossing should get narrower**. This would have been a lengthy process to show experimentally, and as such this was not done due to time constraints. However, Fig 5.7 shows how this would look theoretically at a reduced suspension point.

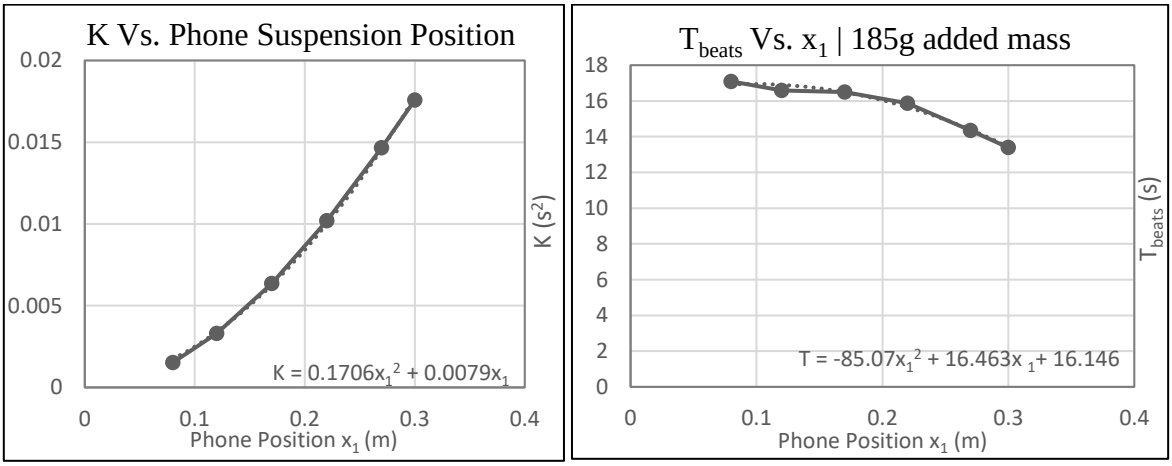

Fig 5.6 | Effects of varied suspension point on cantilever coupling *K* and beat period T_{beats}

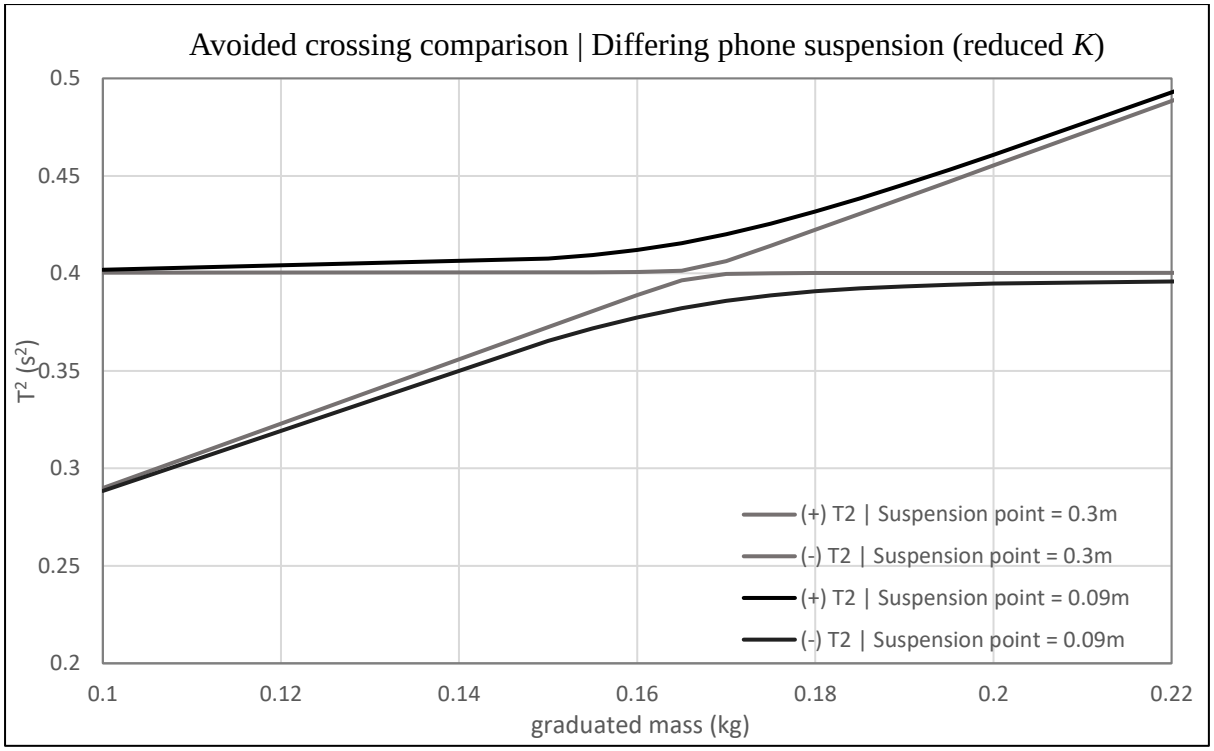

Fig 5.8 | Altered avoided crossing for 0.3m suspension and 0.09m

5.4.2 Investigation of apparent coupling of a double mass-spring system and a single mass-spring system on a cantilever

For no purpose other than to satisfy curiosity, I wanted to explore the dynamics of the previously investigated system with additional complexity, in hopes of finding something interesting. As per Fig 5.9, I added an additional spring-mass system onto the existing setup. I warranted the results of this investigation interesting enough to include in this report.

Consider the following setup in Figure 5.9 and 5.10:

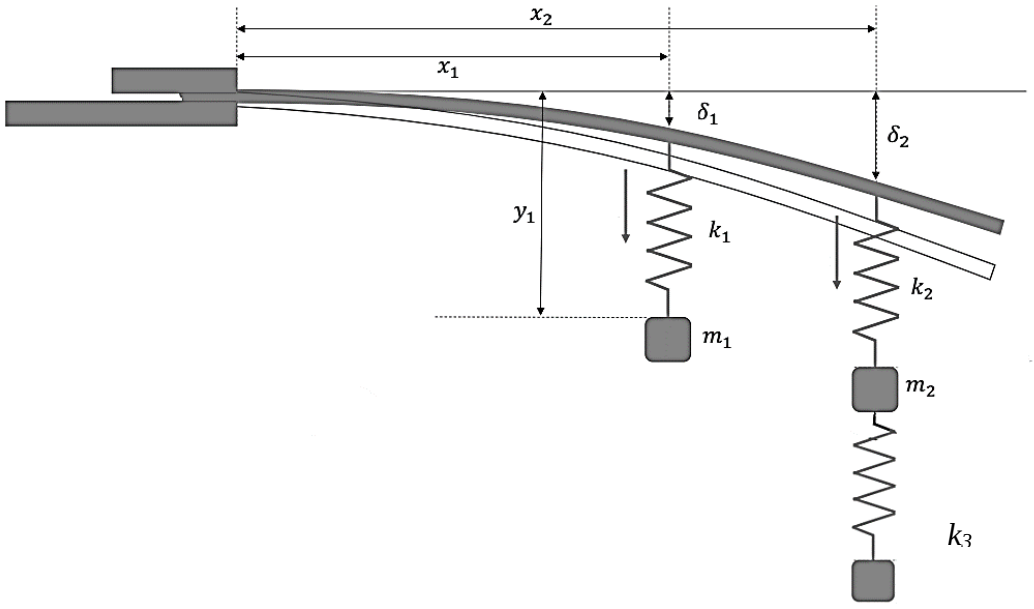

Fig 5.9 | Schematic setup for further investigation

By creating another picture hook/safety pin connector, and borrowing an additional spring from another student, I was able to make the following apparatus to conduct some extra experiments:

Fig 5.10 | New apparatus and experimental setup

There were a number of constraints that limited me from exploring this system thoroughly, for example, being only limited to using the MDF block used for *experiment (c)* as a mass that cannot be altered.

Firstly, I conducted the same experiment as shown in section 5.2, where we varied the mass on the system with all apparatus at fixed suspension points of the cantilever. The setup for this is as shown in Fig 5.10 above.

When reading the FFT spectra for cases individually and plotting them as done previously, we can observe what *appears* to be the making of a similar avoided crossing to that seen for the simpler setup. See Figure 5.11.

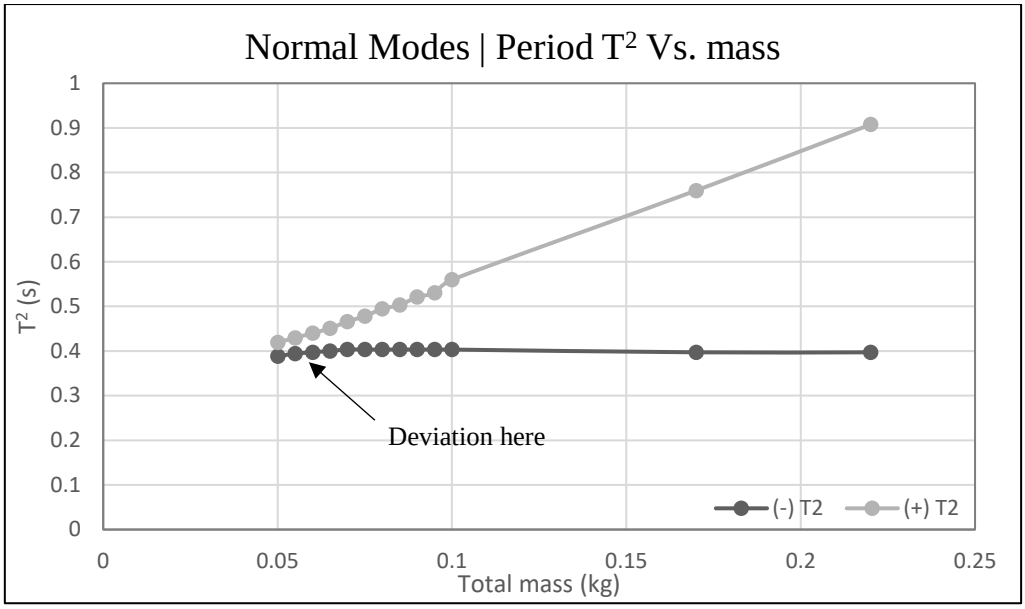

Fig 5.11 | Avoided crossing trends not unlike the previous setup.

m(added) kg	m(incl. holder) kg	Peak 1 Hz	Peak 2 Hz	(+) T^2 s^2	(-) T^2 s^2	splitting s^2
0	0.05	1.5441	1.6052	0.388098	0.41942	0.031322
0.005	0.055	1.5259	1.5929	0.394115	0.429485	0.03537
0.01	0.06	1.5075	1.5869	0.397101	0.440033	0.042932
0.015	0.065	1.4892	1.5808	0.400171	0.450914	0.050743
0.02	0.07	1.4648	1.5747	0.403278	0.466062	0.062784
0.025	0.075	1.4465	1.5747	0.403278	0.477929	0.074651
0.03	0.08	1.4221	1.5747	0.403278	0.49447	0.091192
0.035	0.085	1.4099	1.5747	0.403278	0.503064	0.099786
0.04	0.09	1.3855	1.5747	0.403278	0.520939	0.117661
0.045	0.095	1.3732	1.5747	0.403278	0.530313	0.127035
0.05	0.1	1.3367	1.5747	0.403278	0.55967	0.156392
0.12	0.17	1.1474	1.5869	0.397101	0.759574	0.362473
0.17	0.22	1.0498	1.5869	0.397101	0.907375	0.510274

Tab 5.4 | Experimental Data as per Figure 5.11

Due to apparatus constraints, an extended view of situation was not possible to graph. Had I the equipment to be able to plot this out in it's entirety I would, however I could not build a sturdy and structurally reliable setup to continue this test further. I am assuming the above to be an avoided crossing off of the following basis: **beats can be observed for small added masses**. Judging by how close the supposed avoided crossing is in Figure 5.11, we would expect to begin to see resonance, which is in fact the case as demonstrated in Figure 5.12.

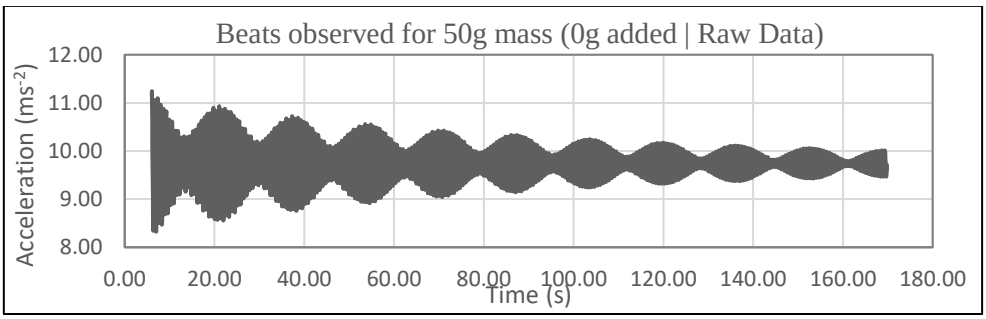

Fig 5.12 | Beats observed with double-spring mass in series

The combined mass of the MDF block and mass holder is approximately 170g, this is almost the point at which we saw perfect resonance in the previous experiment (185g).

Initially, I thought I may have wasted my time doing this, as one would expect (for this example) that as the added mass decreases the more we converge to resonance due to forces from the second spring (bottom one) becoming negligible and we just end up with an effective mass of ~170g, giving rise to the resonance we would observe for the normal setup. However, **we see behaviour for added masses of larger and larger values that indicate an avoided crossing not unlike what we saw previously,** which I find very interesting, especially if we consider that *as we add more mass to the bottom portion of the system; the more the bottom spring contributes to the overall forces*, tending to no longer be a negligible component - and yet we see behaviour as per Figure 5.11.

Side Remark: In PY2107 (Experimental Physics I) we concluded that for a double mass-spring system in series where masses (*m*) and spring constants (*k*) were equal; that the two fundamental modes could be determined as

$$\omega_1^2 = \frac{3+\sqrt{5}}{2}\omega_0^2 \quad \text{and} \quad \omega_2^2 = \frac{3-\sqrt{5}}{2}\omega_0^2 \qquad \text{[4] See Reference}$$

where $\omega_0^2 = \frac{k}{m}$. We also concluded that under these specific conditions (equal masses and spring constants) that the motion was chaotic. Something I attempted to investigate was if we could observe beats in the system under these otherwise chaotic conditions. This investigation has shown that **this cannot be done** with our setup**.** Attempts included:

- Setting the system in oscillatory motion on the cantilever at different lengths
- Adding additional oscillators (mass-spings) to the cantilever at various weights and suspensions points.

An interesting observation was that for some cases where masses were **not** equal, **the double spring system was observed to synchronize at a seemingly faster rate when there was an additional oscillator present on the cantilever** (than when not). This is more of a qualitative argument, as the data collected is not very good as a visual aid in exemplifying this, but it is available in the data files submitted regardless.

Another interesting point of discussion for this setup is regarding the expected modes from theory. For the case where the masses were equal (MDF block mass ≈ 120g), we expect modes (*as per [4]*) at

$$f_1 = \frac{\omega_1}{2\pi} \approx (2\pi)^{-1}\sqrt{\left(\frac{3+\sqrt{5}}{2}\frac{24\ Nm^{-1}}{0.12\ kg}\right)} = \mathbf{3.641\ Hz}$$

$$f_2 \approx (2\pi)^{-1}\sqrt{\left(\frac{3-\sqrt{5}}{2}\frac{24\ Nm^{-1}}{0.12\ kg}\right)} = \mathbf{1.391\ Hz}$$

Figure 5.13 shows that **these modes appear to be altered or simply missing**. In the below Figure, it would not make sense that the frequency at 1.57 Hz corresponds to one of these modes because the phone is isolated on its spring (See Figure 5.10), however it is not unlikely that our calculation may be off by **+0.2 Hz** – meaning that the mode perfectly overlaps with the single spring frequency mode, but I don't think this is the case personally as we have seen avoided crossings in cases like this previously.

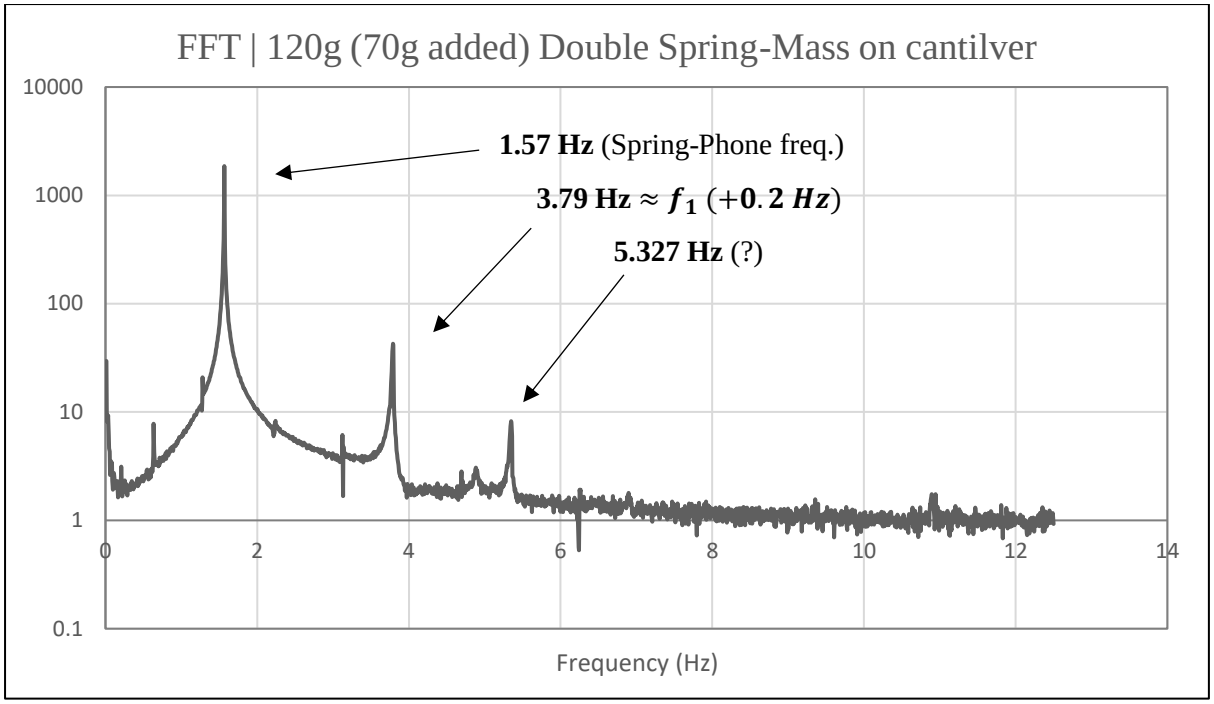

Fig 5.13 | Expected modes potentially missing?

It is disappointing that I did not have the materials to investigate this further. It could be the case that the modes we derived in PY2107 do not apply exactly to this setup and a full re-derivation is required. I say this because there is a mode at **5.327 Hz** that is unidentifiable from theory, but just happens to relate to the other peaks by:

$$\mathbf{1.57\ Hz + 3.79\ Hz = 5.36\ Hz \quad \approx \quad 5.327\ Hz}$$

6. Phone Oscillation Modes and Parametric Resonance (e)

6.1 Theory / Procedure

Nonlinear resonance refers to the phenomenon where an oscillating system responds to an external force or perturbation in a way that is not proportional to the magnitude of the force or perturbation – opposed to linear resonance, where the response of a system to an external force is directly proportional to the magnitude of the force.

Parametric resonance refers to coupling between pendulum motion and vertical oscillatory motion in an elastic pendulum as a result of non-linear resonance. In the setup as shown in Figure 6.1, we can tune the pendulum motion by varying the length of the string. The supplementary material included with the laboratory manual concluded that the non-linear resonance condition for this setup is

$$2\omega_p = \omega_s$$

where ω_p refers to the pendulum angular frequency and ω_s the spring angular frequency. As derived in the supplementary material, the vibration frequencies for the setup as shown in Figure 6.1 can be calculated using

$$\frac{2g}{\omega^2} = l_1 + \frac{{l_1}^2 + {l_2}^2}{2} \pm \sqrt{\left[l_1 - \frac{{l_1}^2 + R^2}{2}\right]^2 + 4l_1 l_2}$$

where l_1 represents the rest length of the string and spring combined, l_2 (in the context of our experimental setup) is the distance from the centre of mass of our phone to where the phone holder attaches to the base of the spring and *R* is the radius of gyration of the smart phone about it's centre of mass.

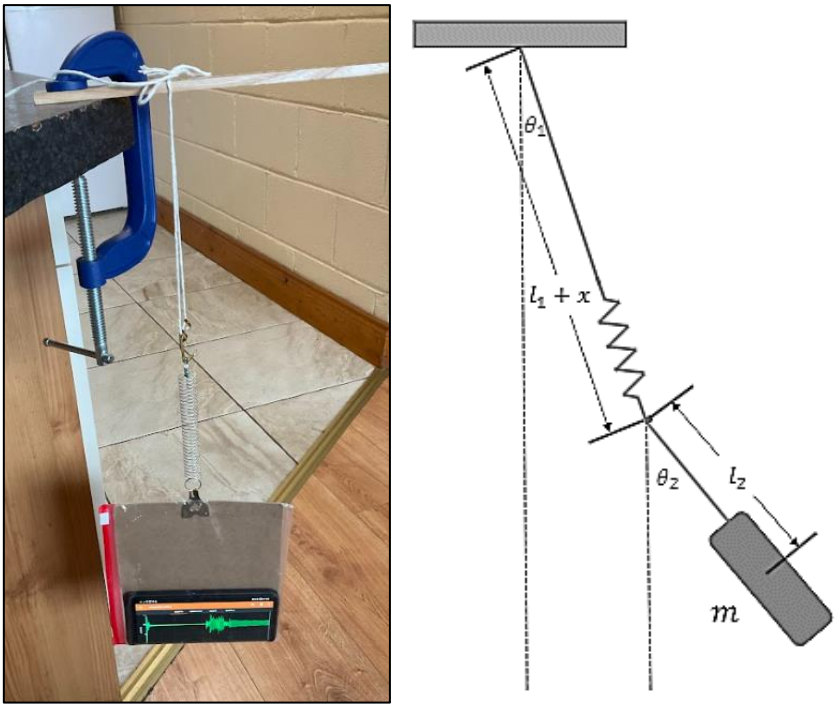

Fig 6.1 | Experimental and schematic setup for experiment (*e*)

The procedure used to obtain the results shown in the remainder of this report is **identical** to the recommended procedure in the lab manual *with one additional measurement* for every run. That is, with the setup as shown in Figure 6.1 with the phone was suspended by a string loop and spring, and for varying lengths of string loop the following measurements were taken:

- Acceleration Spectrum when **phone pulled downwards** from equilibrium (horizontal/pendulum motion minimum) [*labelled as* "(a)" *in filing*]
- Acceleration spectrum when **phone pulled to one side** (along phones length, vertical/spring oscillation minimised) [*labelled as* "(b)" *in filing*]
- Acceleration spectrum when **phone set in torsional oscillation** [*labelled as* "(c)"]
- A *small sample* of acceleration spectrums where phone was pulled to one side such that the **pendulum motion is against the phone face/screen** [*labelled as* "(d)" – these are not analysed for reasons explained, but are provided]

Note: The lab manual procedure specifies measurements for lengths $l_1 + l_2$ of 20cm – 45cm, however for my particular setup the minimum $l_1 + l_2$ was approximately 30cm (string length = 0cm)

6.2 Experimental Data / Analysis

I would like to start with the following observation; for the small few runs where time was spent to measure (d) *("pendulum motion perpendicular to phone face/screen")*, no useful data or conclusions could be drawn from these measurements for a combination of factors.

Firstly, the setup did not allow for steady motion about this axis, as the string-loop axis are not aligned orthogonally to the zip lock bag at rest (see Figure 6.2 for extended context). Secondly,

and more importantly, the **intermediate axis theorem** somewhat prevents oscillations of this type under normal circumstances anyway. As such, the data collected from measurements labelled (d) were of no use other than to provide interesting observation and their collection was abandoned after a few measurements.

Fig 6.2 | Spring loop axis not orthogonal to face of phone/bag

My method of analysis is likely very different to others. Having taken all measurements, I concluded that I personally would find it easier to analyse the extensively large data set and each FFT in the form of animations of the spectra. **I animated the evolution of the visible peaks (FFTs) with respect to the string length** using the data collected**.** I will be referencing these throughout this discussion and as such they are provided in [*'Data'* → *'Part (e)'* → *'Animated Figures'*] to view.

Making these animations provided insights into how the system evolved (and the emerging patterns within) which was likely a faster process than lining them up in spreadsheet for qualitative analysis. The main idea of the animations is that one can change the speed of playback if they like, but also manually scrub through the footage (back and forth) in order to pick out correlating or altered peak positions.

6.3 *Initial Calculations*

According to the equation determined in the supplementary material for the frequency modes

$$\frac{2g}{\omega^2} = l_1 + \frac{{l_1}^2 + {l_2}^2}{2} \pm \sqrt{\left[l_1 - \frac{{l_1}^2 + R^2}{2}\right]^2 + 4l_1 l_2}$$

we require constant values for l_2 and R, which we can calculate. The value of l_1, as per the procedure in the lab manual, is not fixed and corresponds (in this setup) to the addition of the rest length of the spring, l_{spring}, the length of the picture hook, l_{hook}, and the current length of the string loop, l_{string}.

$$l_1 = l_{spring} + l_{hook} + l_{string}$$

l_{spring} can be calculated using Hooke's law and the previously determined spring constant:

$$k_a = (23.4 \pm 0.2) Nm^{-1}; \quad M_{phone} = (237.303 \pm 0.0005) g$$

$$mg = kx \quad \rightarrow \quad M_{phone} a_g = k_a l_{spring}$$

$$l_{spring} = \frac{M_{phone} a_g}{k_a} = \frac{(0.237303\ kg)(9.81\ ms^{-1})}{23.4\ Nm^{-1}}$$

$$\therefore \boldsymbol{l_{spring} = (9.95 \pm 0.09) \times 10^{-2} m}$$

(See Appendix B for error analysis)

l_{hook} was obtained by direct measurement:

$$\boldsymbol{l_{hook} = (0.035 \pm 0.0005) m}$$

Finally, R, the radius of gyration of the phone about its centre of mass, can be obtained from a brief analysis. In experiment (c) we measured the moments of inertia of the smartphone to be

$$I_{pl} = (3.98 \pm 0.04) \times 10^{-4}\ kg\ m^2 = I_y$$

$$I_{ps} = (1.37 \pm 0.08) \times 10^{-4}\ kg\ m^2 = I_x$$

where I_{pl} is the moment about it's "long" side length (y-axis) and I_{ps} about it's "short" side length (x-axis). From literature (and the supplementary material provided) it is know that we can approximate the third moment of inertia about the z-axis to be

$$I_z \approx I_x + I_y$$

$$\therefore \boldsymbol{I_z = (5.35 \pm 0.12) \times 10^{-4}\ kg\ m^2}$$

Since $I = MR^2$, we can finally conclude that

$$R = \sqrt{\frac{5.35 \times 10^{-4}\ kg\ m^2}{0.237303\ kg}} = 0.0475\ m$$

$$\therefore \boldsymbol{R = (0.0475 \pm 0.0005)\ m}$$

(See Appendix B for error analysis)

l_2 can be determined by direct measurement. We concluded in experiment (c) that **the smart phone in use has an approximately uniform centre of mass** from the comparison in gyration radii to the uniform MDF block. As such, we can accurately make the following analysis (See Figure 6.3):

$$l_2 = l_{hook} + l_c$$

We already determined $l_{hook} = (0.035 \pm 0.0005) m$. The exact measurement l_c, as per Figure 6.3, was taken using the provided measuring tape and double checked with the half meter stick:

$$\boldsymbol{l_2 = (0.1685 \pm 0.0005)\ m}$$

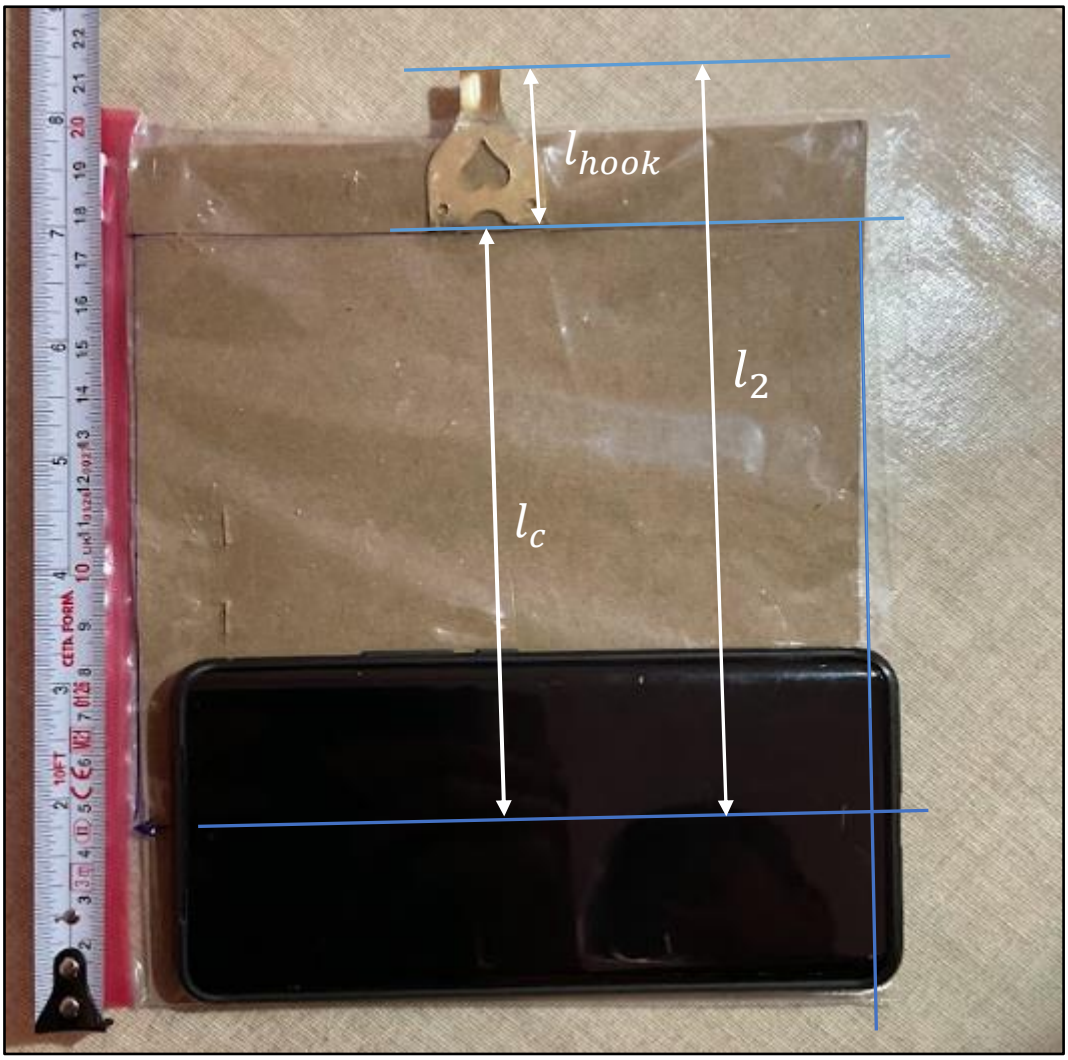

Fig 6.3 | Determination of l_2

In summary:

$$R = (0.0475 \pm 0.0005)\ m$$

$$l_2 = (0.1685 \pm 0.0005)\ m$$

$$l_1 = l_{spring} + l_{hook} + l_{string}$$

where $l_{spring} = (9.95 \pm 0.09) \times 10^{-2} m$ *and* $l_{hook} = (3.5 \pm 0.05) \times 10^{-2} m$

6.3.1 FFT Observations and Analysis

The first observation is that the **torsional data held no additional useful information about the system** in question, other than the fact that the frequency of torsional oscillations was related to the length of the string. Otherwise, We see the same pattern and peaks as investigated in experiment (c), which do not tend to appear in the other data sets. This would lead one to believe that **torsional oscillations in this setup are not affected by parametric or non-linear resonance**.

We can calculate from theory where we expect to see resonance in the data. From the non-linear resonance condition we expect to see parametric resonance when

$$2f_p = f_s$$

where $f_s = \sqrt{\frac{k_a}{M_{phone}}}/2\pi$. Using the parameters as determined earlier:

$$f_s = \frac{\sqrt{\frac{23.4\ Nm^{-1}}{0.237303\ kg}}}{2\pi} = 1.58\ Hz$$

which simply allows to conclude that we should parametric resonance at

$$f_p = \frac{1.58\ Hz}{2} = 0.79\ Hz$$

Using the values obtained in the previous section we can fill out the following table for the measurement taken of the various pendulum lengths (recognising that $f = \frac{\omega}{2\pi}$):

			THEORY		
l_{string} m	l_1 m	l_1+l_2 m	(+) f_p Hz	(-) f_p Hz	
0.02	0.15453	0.32303	0.86775	6.3004	
0.057	0.19153	0.36003	0.82368	5.962	Expect Parametric Resonance
0.084	0.21853	0.38703	0.79536	5.7802	
0.11	0.24453	0.41303	0.77064	5.6396	
0.138	0.27253	0.44103	0.74638	5.5156	
0.195	0.32953	0.49803	0.70326	5.3235	
0.198	0.33253	0.50103	0.70119	5.3151	
0.232	0.36653	0.53503	0.67893	5.2286	
0.258	0.39253	0.56103	0.66325	5.1719	
0.283	0.41753	0.58603	0.64914	5.1236	
0.305	0.43953	0.60803	0.63744	5.0854	
0.352	0.48653	0.65503	0.61441	5.0148	
0.394	0.52853	0.69703	0.5958	4.9617	
0.454	0.58853	0.75703	0.5719	4.8984	

Tab 6.1 | Expected modes of vibration as per theory – See spreadsheets for more.

As such for the measurements taken, we expect to parametric resonance at an $l_1 + l_2$ of ~*39cm* with a corresponding l_{string} of ~*9cm*.

Observation: The FFTs of $l_{string} = 0.084m$ and $0.057m$ are the only two to mutually share every significant visible peak (due to parametric resonance - See Figure 6.4):

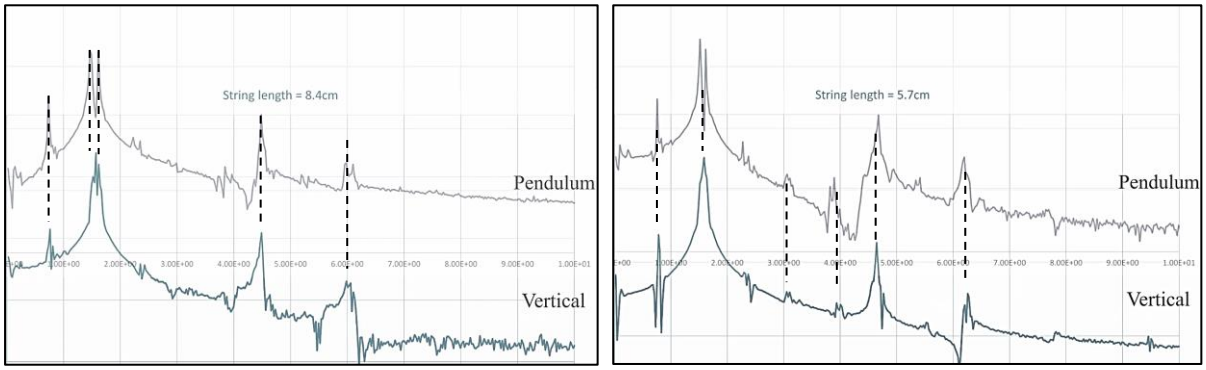

Fig 6.3 | Parametric Resonance Observed in expected FFTs [Screenshots From Animation 6.1]

LEFT: $l_{string} = 0.084m$ | RIGHT: $l_{string} = 0.057m$

Taking a look at the raw sensor data for $l_{string} = 0.057m$, we can observe interesting behaviour, which has been differentiated into corresponding events (See Figure 6.4):

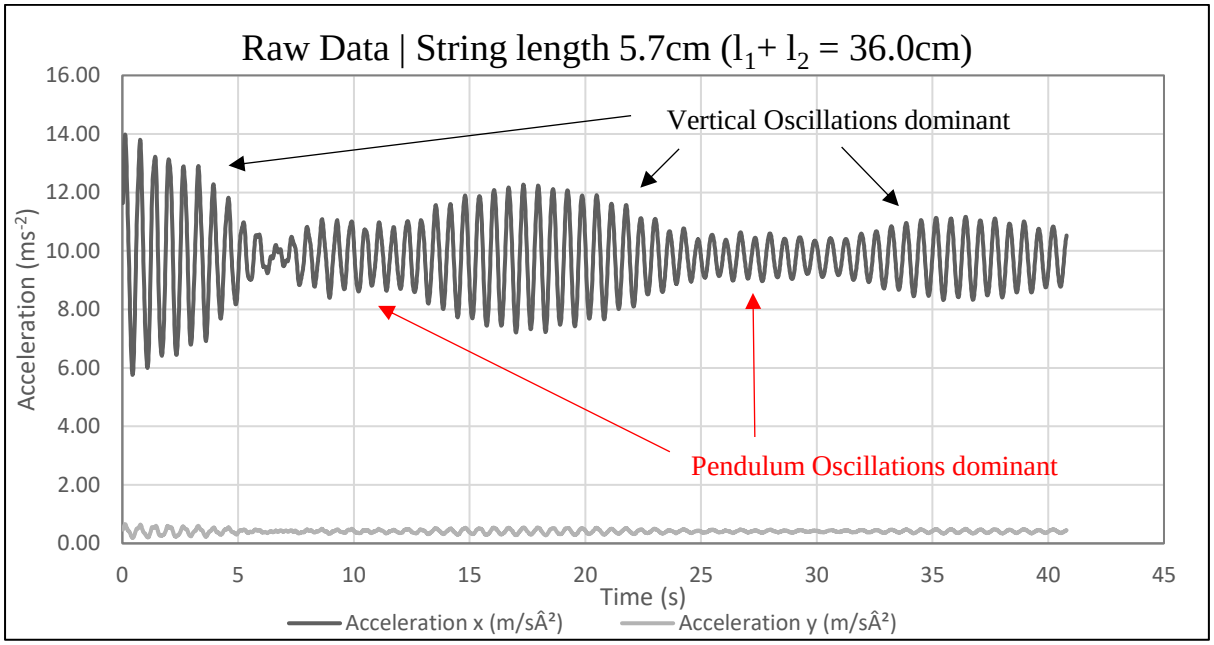

Fig 6.4 | Parametric Resonance as Observed in Raw Data

In this graph, we should really expect something like this (Figure 6.5) between the x and y data:

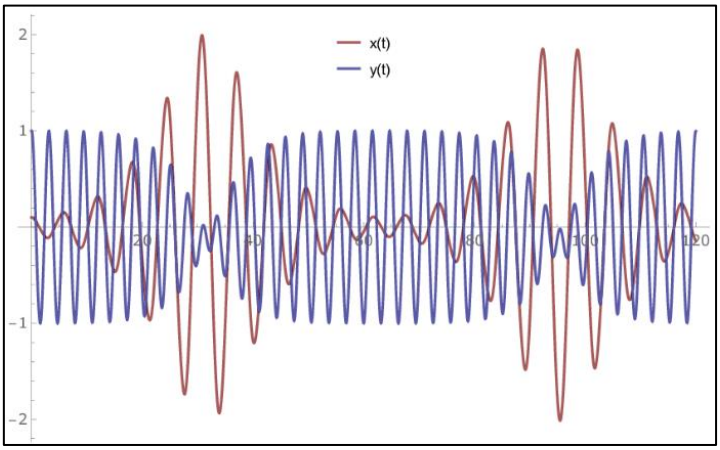

Fig 6.5 [5] | Parametric Resonance in a perfect 2D system | See Reference [5] for Source.

We do not observe this because we are not working in an ideal 2D environment, and as mentioned previously motion in just 2 axes was likely impossible as the spring and loop axis are not aligned orthogonally to zip lock bag (See earlier discussion).

Compare this now to a pendulum length where we **should not expect resonance**, say $l_{string} = 0.305m$. Taking a look at Figure 6.6, we do not see mutual peaks under 2 Hz, and some significant peaks after that also do not align mutually.

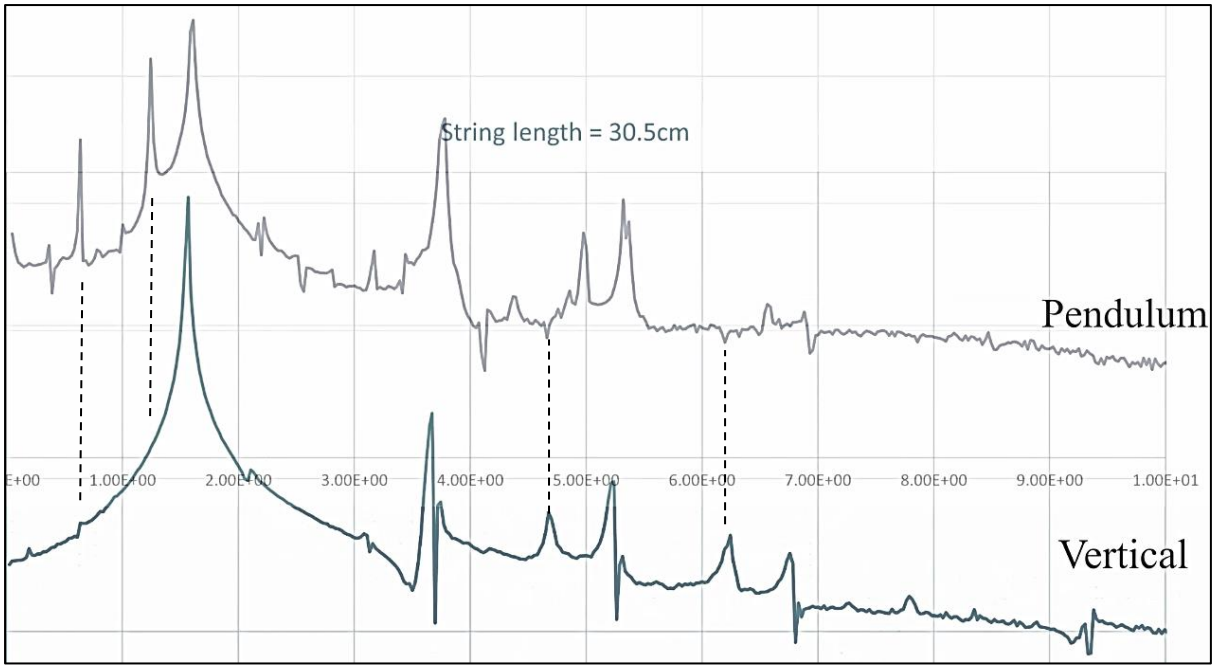

Fig 6.6 | $l_{string} = 0.305m$ [Screenshot From Animation 6.1] | dotted ines do not align to mutual peaks

If we look at the raw sensor data for this run, we do not observe the same behaviour as the previous example:

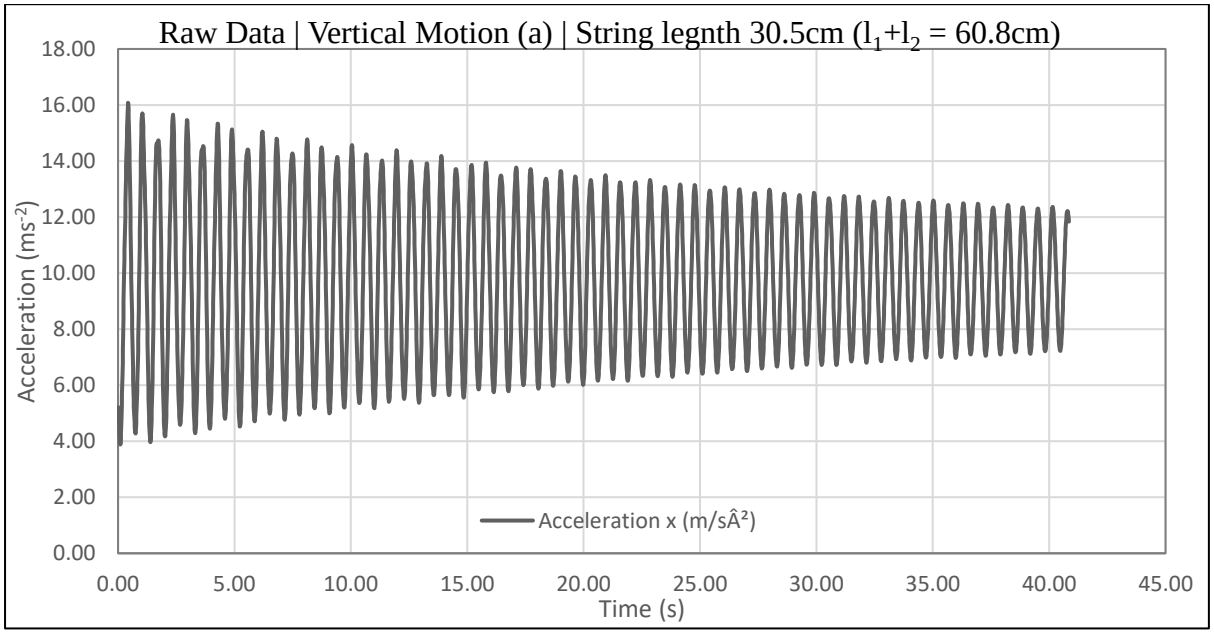

Fig 6.7 | $l_{string} = 0.305m$ | Raw Data | There is no resonance to be seen in the raw data, as expected from theory and Tab 6.1.

I would implore the reader to view **Animation 6.1** for an extended context of how the system's modes of vibration evolve with respect to the string-loop length. As per the above discussion, **we have observed parametric resonance under the expected conditions according to theory.**

Drawing attention now to the spectra for the pendulum motion data set, there are two distinct peaks that move in frequency as the string length increases. The peaks, as shown in Figure 6.8, are clearly a product of the pendulum motion as **they only appear in the vertical motion**

spectra for cases of parametric resonance. The peaks also have a frequency ratio 2:1 (one is consistently at half the frequency of the other). Please see **Animation 6.2** and **Figure 6.7** for visualisation of this.

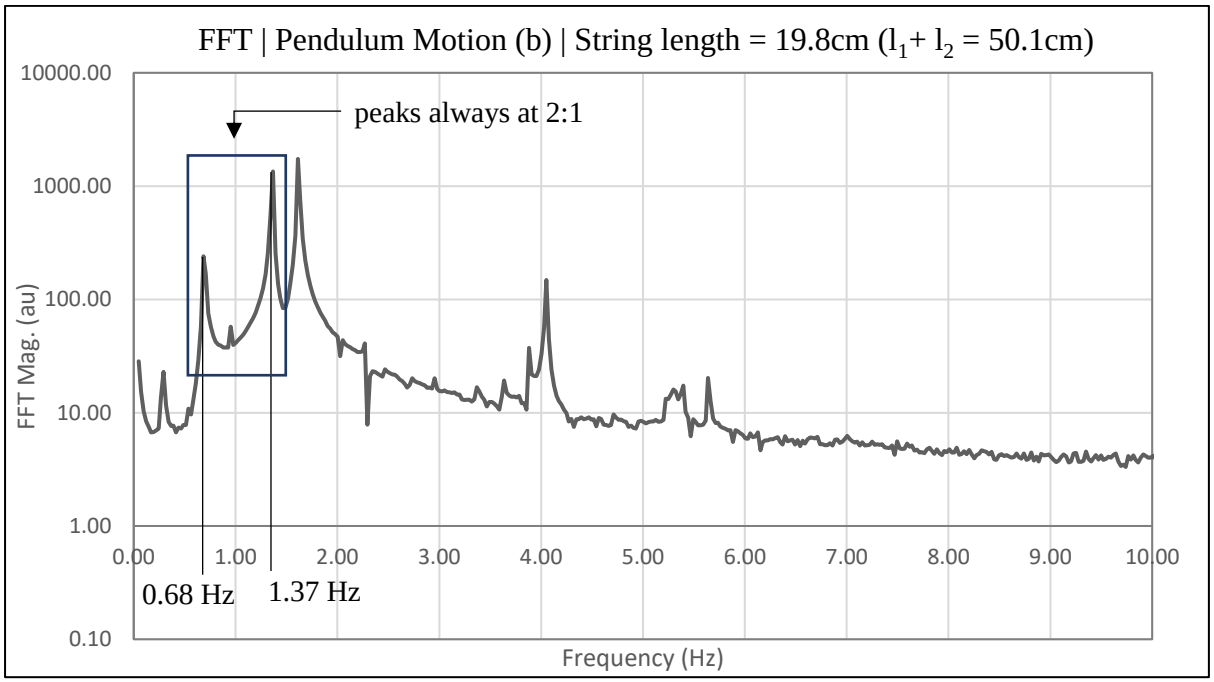

Fig 6.8 | $l_{string} = 0.198m$ | FFT | Peaks are at Ratio 2:1

We know from direct comparison to Tab 6.1 that the lower peak (the half frequency peak) is a double pendulum mode. The 2nd peak is difficult to identify in the raw data, but from theory we know this to be the "**driving" frequency**, which is a result of the **driving force** of the pendulum:

$$D \approx \frac{ga^2}{4}[1 - 3\cos(2\omega_p t)]$$

The supplementary material states "Note that the frequency of the driver is $2\omega_p$, twice the pendulum frequency".

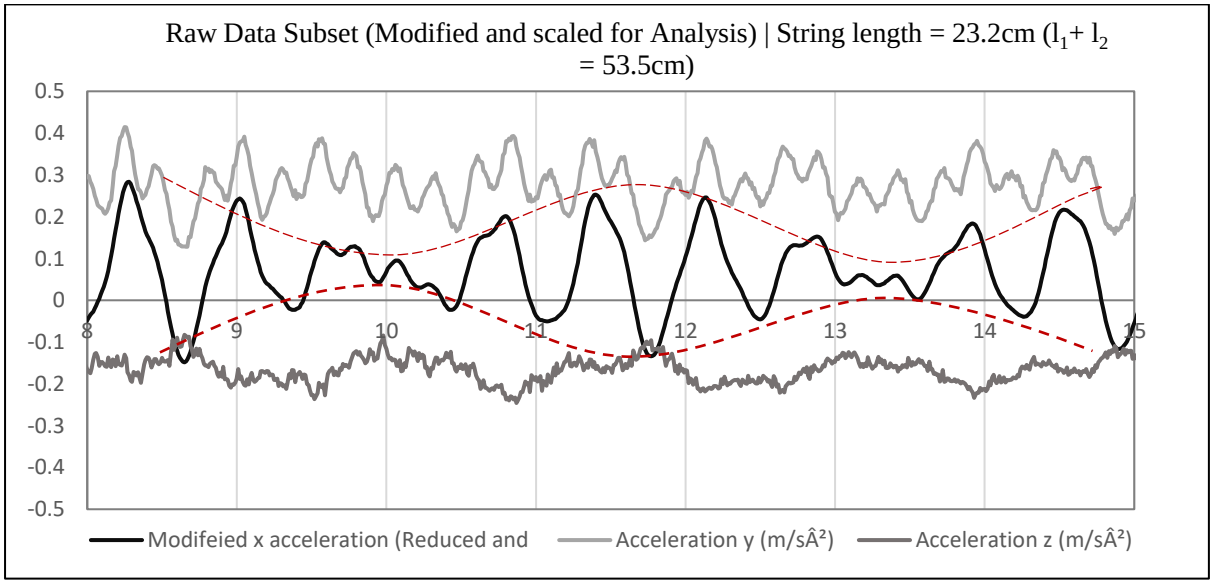

Fig 6.9 | $l_{string} = 0.232m$ | Raw Data | Rough calculation of beat period from knowing f_s

From Figure above we can determine the period of beats for a particular measurement to be approximately 0.314 Hz.

$$\frac{f_s}{\#oscillations\ per\ beat} \approx \frac{1.57\ Hz}{5} \approx 0.314\ Hz$$

This is a peak present in the produced FFT:

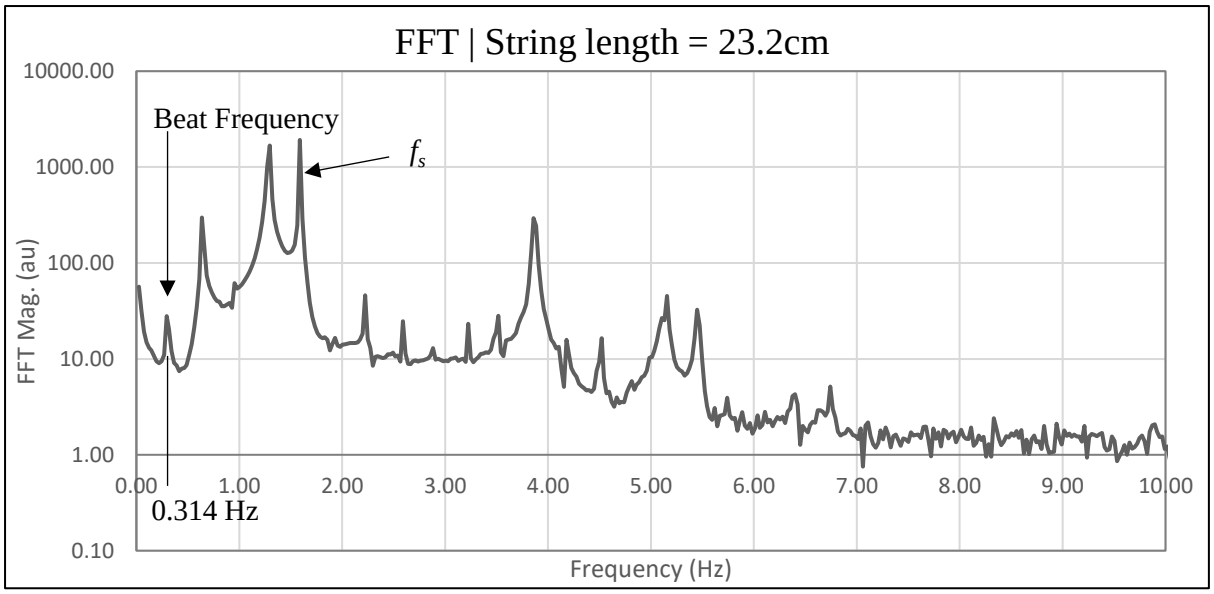

Fig 6.10 | $l_{string} = 0.198m$ | FFT | Peaks are at Ratio 2:1

In Animation 6.2, this peak can be seen to increase in frequency as string length increases (it's very, very subtle and not always present), which is a trend that is also present in the raw data, **the observed beat frequencies (for pendulum oscillations) increase as string length increases** (as we move away from resonance).

This is analogous to another observation, **where the difference between the 2nd (larger) peak and the spring-mass frequency peak is approximately equal to the beat frequency observed.**

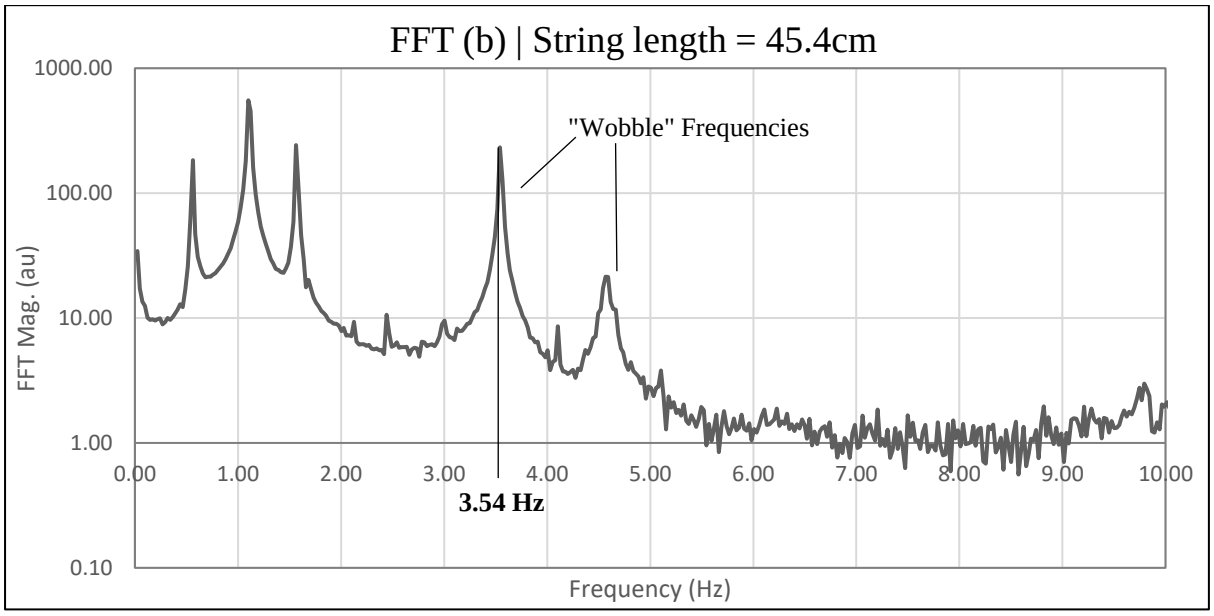

Fig 6.11 | $l_{string} = 0.198m$ | FFT | Peaks are at Ratio 2:1

The last two big peaks at the higher frequencies above are evidently 'wobble' frequencies, high frequency motion from sporadic pendulum motion of the phone/bag. Evidence of this can be seen in Figure 6.12, where **a subset of the pendulum motion can be seen have the higher frequency ripple within**:

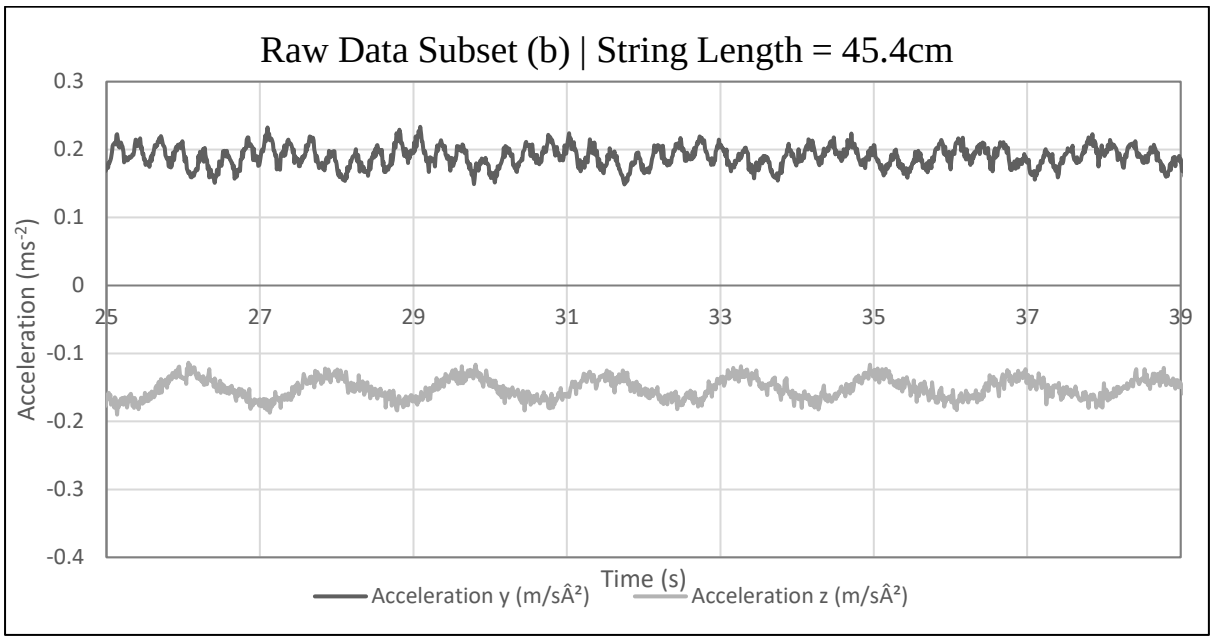

Fig 6.12 | $l_{string} = 0.454m$ | Raw Data | Wobble evident in pendulum motion

Physical intuition would tell us that supposed 'wobble' frequencies would in fact be higher due to the nature of the spring forces present (always attempting to restore the pendulum to a straight, steady state) and that these would decrease in frequency naturally as the pendulum gets longer (the torque that would be required to restore effectively would become more significant).

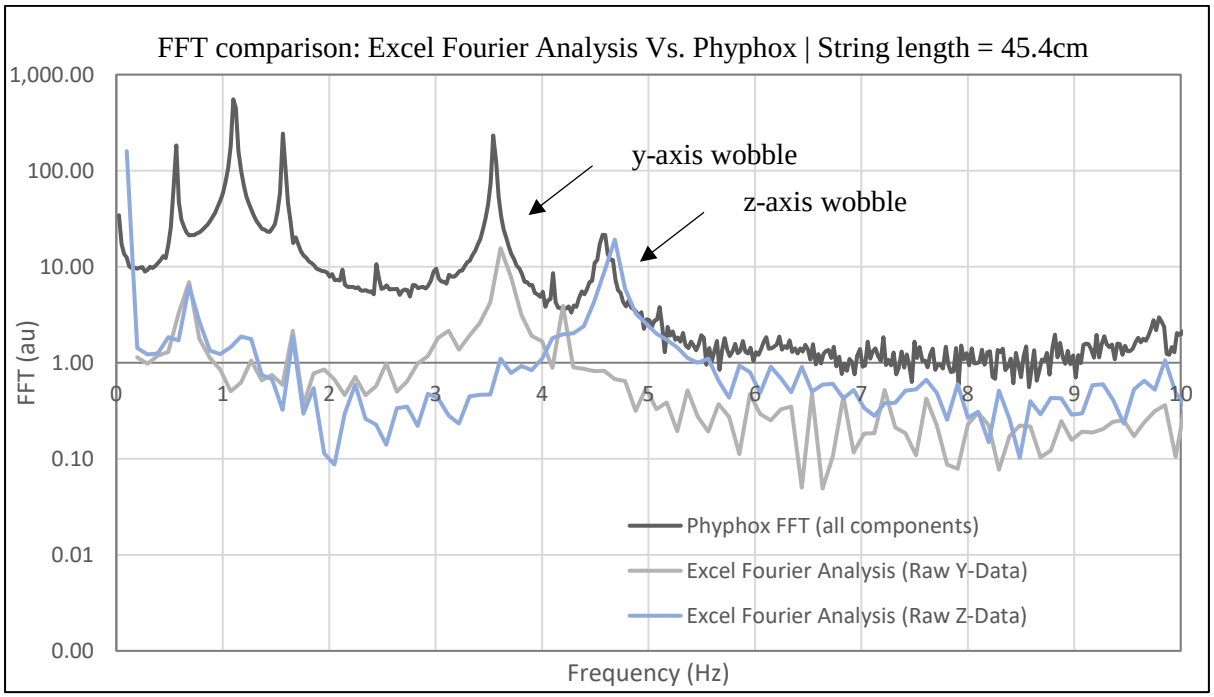

Fig 6.13 | $l_{string} = 0.454m$ | Raw Data | Wobble evident in pendulum motion

Using **Excel Fourier Analysis** tool on Raw Data of both axes (See above Figure); we can see that the supposed wobble peaks match up. This is rather definitive, and proves intuition correct.

Although I could not explicitly locate and verify the higher frequency wobbles, they must be related; **Animation 6.3** (viewing recommended) demonstrates many of these wobble frequencies and how the differences between them remain constant for individual string lengths in vertical motion. However, **depending the type of motion the system was initially set in, the wobble frequencies evolve differently**. I cannot conclude why this is the case, but it may have to do with differences in the spring restoring force as a result of more significant pendulum motion – **perhaps there are other non-linear contributors at play here**.

Regardless, we know that the peaks in both cases are related, as when we observe parametric resonance, the peaks align directly (See earlier Figure 6.6 and Animation 6.1)

Verdict: Following this lengthy analysis, we can conclude the following identities for the various peaks observable in the FFTs produced:

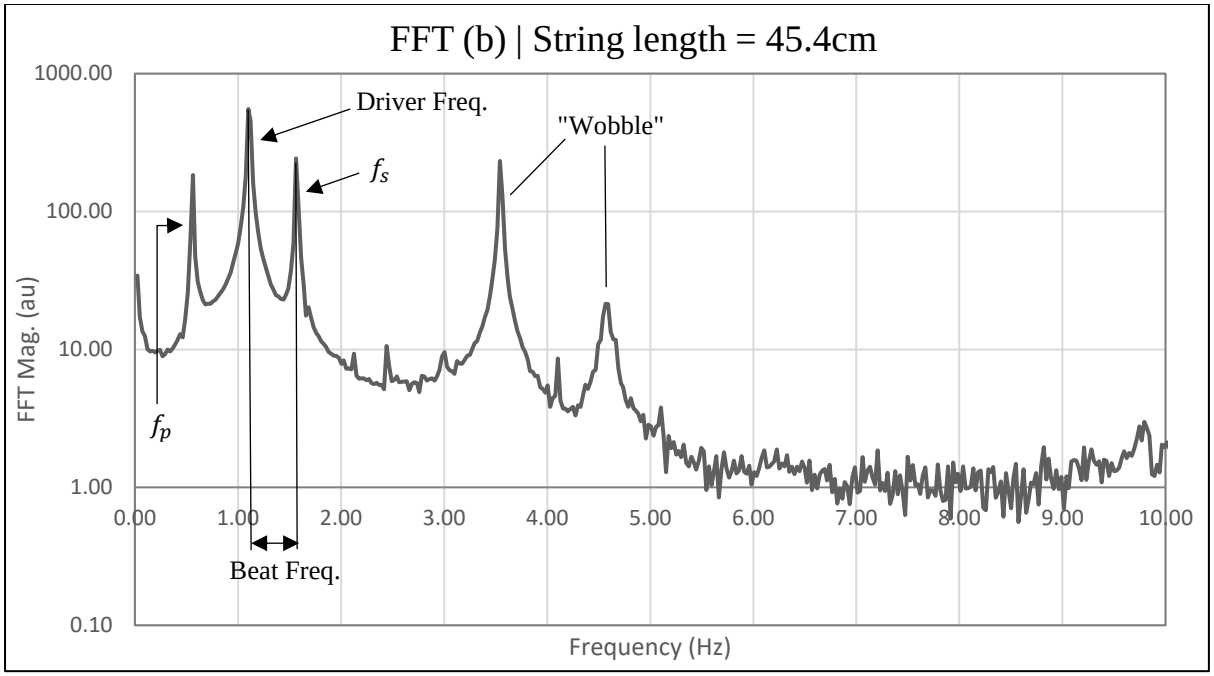

Fig 6.14 | $l_{string} = 0.454m$ | Raw Data | All peaks identified for all cases.

7. Conclusions

Completing these experiments have, personally, provided an appreciation of the true complexity of coupling. The vast amount of analysis that can be done on a seemingly simple setup is jarring. This report has shown that an experimentalist, with simple everyday items, can make a thorough and justified analysis of complex, dynamic systems, and can do so with technology available in most of the population's pocket.

In conclusion to the technical material showcased, the experimental setups for each experiment can certainly be improved and refined further. For example, the raw sensor data at parametric resonance could have been more ideal, the trends/beats present (specifically in Fig 6.4) may have been difficult to quantify/identify under increasingly less ideal conditions. There are other cases where the imperfect nature of the setup gave way to interesting observations and events, such as the wobble frequencies later in experiment (e).

I would certainly be interested in exploring the ideas and methods investigated throughout even further if given the opportunity and time to. Overall, this report hopefully serves as a relatively grounded and reliable investigation into coupled oscillation.

References

[1] Definition by Britannica, Source: https://www.britannica.com/science/beat-waves

[2] Typical Young's Modulus of Fir according to AmesWeb, Source: https://amesweb.info/Materials/Youngs-Modulus-of-Wood.aspx

[3] Honor 50 Teardown Source: https://min.news/en/tech/5c48ea74cb3db833bb28d61f24cb7f15.html

[4] PY2107 Lab 2 Manual – 'Coupled Spring Oscillation'.

[5] 'Parametric Resonance in a system with 2 modes', Figure Source: https://www.researchgate.net/figure/An-example-of-a-parametric-resonance-in-a-closed-system-with-two-modes-The-frequencies_fig1_325282791

Appendices

A. Derivations

1. **Fourier Transform of a Damped Exponential**

$$z(t) = e^{-\gamma t}\cos(2\pi\nu t)$$

$$P(f) = \left|\int_0^\infty e^{2\pi f i} e^{-\gamma t}\cos(2\pi\nu t)\,dt\right|$$

$$= \frac{1}{2\pi}\left|f - \nu + \frac{\gamma i}{2\pi}\right|^{-1}$$

$$= \left(2\pi\sqrt{(f-\nu)^2 + \left(\frac{\gamma}{2\pi}\right)^2}\right)^{-1}$$

$$\equiv \frac{1}{2\pi\sqrt{(f-\nu)^2 + \left(\frac{\gamma}{2\pi}\right)^2}}$$

B. Error Analysis for Experiment (e)

Uncertainty of l_{spring}:

$$\frac{\Delta l_{spring}}{l_{spring}} = \frac{\Delta M_{phone}}{M_{phone}} + \frac{\Delta k_a}{k_a} + \frac{\Delta g_a}{g_a}$$

$g_a = 9.814 ms^{-2}$ *(in Ireland) with an uncertainty/variation of* ± 0.0005

$$\frac{\Delta l_{spring}}{l_{spring}} = \frac{0.0005}{237.303} + \frac{0.2}{23.4} + \frac{0.0005}{9.814} = 0.0086$$

$$\rightarrow \Delta l_{spring} = (0.0086)(0.0995\ m) = 0.0009$$

$$\therefore l_{spring} = (9.95 \pm 0.09) \times 10^{-2} m$$

Uncertainty of R:

$$\frac{\Delta R}{R} = \frac{1}{2}\left(\frac{\Delta I_z}{I_z} + \frac{\Delta M_{phone}}{M_{phone}}\right)$$

$$\frac{\Delta R}{R} = \frac{1}{2}\left(\frac{0.12}{5.35} + \frac{0.0005}{237.303}\right) = 0.01122$$

$$\rightarrow \Delta R = (0.01122)(0.0475\ m) = 0.000533\ m$$

$$\therefore R = (0.0475 \pm 0.0005)\ m$$